

Relatively young thick discs in low-mass star-forming late-type galaxies

Natascha Sattler^{1,2*}, Francesca Pinna^{3,4,1**}, Sebastien Comerón^{4,3}, Marie Martig⁵, Jesus Falcón-Barroso^{3,4}, Ignacio Martín-Navarro^{3,4}, and Nadine Neumayer¹

¹ Max Planck Institute for Astronomy, Königstuhl 17, D-69117 Heidelberg, Germany

² Astronomisches Rechen-Institut, Zentrum für Astronomie der Universität Heidelberg, Mönchhofstraße 12-14, D-69120 Heidelberg, Germany

³ Instituto de Astrofísica de Canarias, Calle Vía Láctea s/n, E-38205 La Laguna, Tenerife, Spain

⁴ Departamento de Astrofísica, Universidad de La Laguna, Av. del Astrofísico Francisco Sánchez s/n, E-38206, La Laguna, Tenerife, Spain

⁵ Astrophysics Research Institute, Liverpool John Moores University, 146 Brownlow Hill, Liverpool, L3 5RF, UK

October 10, 2024

ABSTRACT

Aims. We aim to trace the evolution of eight edge-on star-forming disc galaxies through the analysis of stellar population properties of their thin and thick discs. These galaxies have relatively low stellar masses (4×10^9 to $6 \times 10^{10} M_{\odot}$).

Methods. We use Multi-Unit Spectroscopic Explorer (MUSE) observations and full-spectrum fitting to produce spatially resolved maps of ages, metallicities and [Mg/Fe]-abundances and extract the star formation histories of stellar discs.

Results. Our maps show thick discs that are on average older, more metal-poor and more [Mg/Fe]-enhanced than thin discs. However, age differences between thin and thick discs are small (around 2 Gyr) and the thick discs are younger than previously observed in more massive and more quiescent galaxies. Both thin and thick discs show mostly sub-solar metallicities, and the vertical metallicity gradient is milder than previously observed in similar studies. [Mg/Fe] differences between thick and thin discs are not sharp. The star formation histories of thick discs extend down to recent times, although most of the mass in young stars was formed in thin discs.

Conclusions. Our findings show thick discs that are different from old quiescent thick discs previously observed in galaxies of different morphologies and/or different masses. We propose that thick discs in these galaxies did not form quickly at high redshift, but slowly in an extended time. Also, the thin discs formed slowly, however, a larger mass fraction was created at very recent times.

Key words. galaxies: spiral – galaxies: structure – galaxies: star formation – galaxies: evolution

1. Introduction

A galaxy disc can have multiple disc components that have different thicknesses. Usually two components called thin and thick discs are formed (Burstein 1979; Gilmore & Reid 1983; Yoachim & Dalcanton 2006; Comerón et al. 2018). The former have a higher surface brightness and dominate the midplane region, while the latter are not as bright and dominate at larger heights. The vertical structure of discs can be best studied when they are seen edge-on. Thin and thick discs in external galaxies are usually defined geometrically, by selecting regions at different heights from the midplane (Yoachim & Dalcanton 2006). They also differ in their kinematics, as well as in their stellar populations. Thick discs usually have higher velocity dispersions and mostly show older, more metal-poor and α -enhanced stellar populations than thin discs (e.g. Yoachim & Dalcanton 2008a; Comerón et al. 2015; Kasparova et al. 2016; Pinna et al. 2019b,a; Scott et al. 2021; Martig et al. 2021; Sattler et al. 2023; Pinna et al. 2024). Furthermore for galaxies with circular velocity $> 90 \text{ km s}^{-1}$, they are typically less massive than thin discs but for galaxies with circular velocity $< 90 \text{ km s}^{-1}$, the thin-to-thick disc mass ratios can be lower than one (Yoachim & Dalcanton 2006;

Comerón et al. 2011, 2012, 2019).

Differences in stellar kinematics and populations indicate that thick and thin discs had a different history. The formation of thick discs can be explained by multiple different processes. They can be born already thick through gas-rich mergers (Brook et al. 2004), during which the stars in the thick disc are formed in a turbulent phase at high redshift. They can form through instabilities in the disc (Bournaud et al. 2009) leading to strong stellar scattering. Instabilities of internal origin would result in a thick disc having a constant scale height over all galactocentric radii (Bournaud et al. 2009). In addition, thick discs may form from a previously settled thin disc, that gets dynamically heated by minor mergers (Quinn et al. 1993). This scenario would lead to a flaring thick disc (Bournaud et al. 2009). Furthermore, the accretion of stars from satellite galaxies can build a thick disc structure (Abadi et al. 2003). The stellar accretion might leave retrograde moving stars in the thick disc, which can contribute to a high velocity dispersion (Yoachim & Dalcanton 2008b). Thin discs however are thought to form mainly in-situ. Thereby, large amounts of gas can be provided by gas-rich galaxy mergers or gas accretion along the filaments of the intergalactic medium, which can fuel an extended star formation with a long chemical enrichment to metal-rich and α -poor stars (Gallart et al. 2019;

* e-mail: n.sattler@stud.uni-heidelberg.de

** e-mail: francesca.pinna@iac.es

Martig et al. 2021; Conroy et al. 2022). An extended chemical enrichment only happens after subsequent generations of stars pollute the interstellar medium with their metals. The first high-mass stars, which originally formed from metal-poor gas (Mo et al. 2010), exploded as core-collapse supernova and left some α -elements (e.g. magnesium and oxygen) in the interstellar medium (e.g. Worthey et al. 1992; Mo et al. 2010; Peletier 2013). From this more α -enriched gas, new generations of stars are formed. The enrichment with heavy elements (e.g. iron and nickel) mostly happens when stars explode as type Ia supernova, whose progenitors have a much longer lifetime than those of core-collapse supernova. This causes a delay in the production of iron with respect to α -elements. Therefore, unless they form from recently accreted, pristine gas, the youngest stars which are primarily located in the thin disc have a lower $[\alpha/\text{Fe}]$ -abundance, because they form from slowly evolved gas that contains a larger amount of heavier metals, making them generally more metal-rich.

All these different formation mechanisms of thin and thick discs can be combined to explain the build-up of observed galaxies (e.g. Comerón et al. 2016; Pinna et al. 2019b,a; Santucci et al. 2020; Martig et al. 2021). In Comerón et al. (2014), it was suggested that the thin disc is forming after the build up of the “dynamically hot” component (which includes the thick disc and a central mass concentration). Especially in low-mass galaxies, the “dynamically cold” component (which includes the thin disc and molecular gas) has enough gas to produce a thin disc in the future that is as massive, in relative terms, as current thin discs in high-mass galaxies that have exhausted most of their gas already. Therefore, even if the mass ratio of thick and thin disc varies as function of galaxy mass, the mass ratio of dynamically hot and cold components stays roughly constant. Moreover, cosmological simulations of Milky Way-sized galaxies (Martig et al. 2012; Grand et al. 2017) are also used to study the growth of discs. These show that a thin disc is often present since the earliest evolutionary phase and grows continuously “inside-out” (Pinna et al. 2024). This inside-out process is thought to describe the mass assembly of galaxies with a mass higher than $10^{10.5} M_{\odot}$ (e.g. Pérez et al. 2013; Pan et al. 2015) and can be traced by a negative radial age gradient with older stars in the central region and younger stars in the outskirts (Pérez et al. 2013). In contrast, galaxies with a mass lower than $10^{10} M_{\odot}$ are proposed to form from an “outside-in” process that would leave younger stars in the center and older stars in the outskirts and can thus be traced by a positive radial age gradient (Zhang et al. 2012; Pan et al. 2015).

Distinct thin and thick discs have been identified in numerous galaxies. For example in Yoachim & Dalcanton (2006), 32 out of 34 edge-on galaxies host a thick disc, while in Comerón et al. (2018) 124 out of 141 galaxies can be separated into two large-scale disc structures. Also, the Milky Way is known to own multiple disc structures (Gilmore & Reid 1983). In the solar neighborhood, older, more metal-poor and α -enhanced stars are found at larger distances from the midplane (Gilmore & Wyse 1985; Ivezić et al. 2008; Schlesinger et al. 2012; Casagrande et al. 2016). Radial gradients in age and $[\alpha/\text{Fe}]$ are observed in the Milky Way geometric thick disc (Minchev et al. 2015; Martig et al. 2016; Hayden et al. 2017; Queiroz et al. 2020; Gaia Collaboration et al. 2022). The outer thick disc is dominated by younger stars (around 5 Gyr) that are α -poor, whereas the inner thick disc is older (around 9 Gyr) and more enhanced in α -elements. These radial gradients may result from different formation processes for the inner and outer thick disc, where the inner thick disc is formed already thick at high redshift,

while the outer thick one is continuously growing and external perturbations bring young and α -poor stars in the outer thick disc (Minchev et al. 2015). Otherwise, radial gradients may also emerge from the flaring of the outer region of the thin disc as shown for lenticulars (e.g. Pinna et al. 2019b,a) and Milky Way-mass spiral galaxies (Pinna et al. 2024).

Due to the limited amount of spectroscopic data, it is still unclear whether these processes mentioned above truly describe the formation of the Milky Way and if they can also be applied to external galaxies. There are a few long-slit studies in which the stellar kinematics and stellar populations for the thin and thick discs of edge-on galaxies were analyzed (e.g. Yoachim & Dalcanton 2008b,a; Katkov et al. 2019; Kasparova et al. 2016, 2020). The studies of Yoachim & Dalcanton (2008a,b) provided stellar and gaseous kinematic measurements of nine edge-on late-type galaxies, as well as luminosity-weighted stellar ages and metallicities for their thin and thick discs. The thick discs in their sample show kinematics favoring an accretion origin for thick disc stars. Moreover, they show an old stellar population between 4 to 10 Gyr, while the thin discs are overall younger with a strong negative radial age gradient. In Kasparova et al. (2016), deep spectra of thick discs in three edge-on S0 galaxies were obtained. Two of these galaxies show stellar populations with similar properties ($[\text{Fe}/\text{H}] \sim -0.2$ to 0.0 dex and ages around 4-5 Gyr) for both disc components, while the third one shows only one old (thick) disc component.

However, with the use of integral-field spectroscopy, stellar properties such as kinematics and populations can be mapped spatially in a continuous way, including the transition region between thin and thick discs, and provide detailed insights into the structure of extragalactic discs. Several studies have already been done on bright edge-on S0 galaxies (Comerón et al. 2016; Guérou et al. 2016; Pinna et al. 2019b,a). The quiescent galaxies in Comerón et al. (2016); Pinna et al. (2019b,a) showed very old and metal-poor thick discs (which are also α -enhanced in Pinna et al. 2019b,a), suggesting their short and fast formation at high redshift. Also, Pinna et al. (2019b,a) detected a subdominant but significant, potentially accreted component in the stellar populations of three lenticular galaxies in the Fornax cluster. The study of faint thick discs in spiral galaxies is more challenging because of their low surface brightness and large amounts of gas (producing striking emission lines) and dust making it hard to perform a detailed analysis. The first attempt on spiral galaxies was done with VIMOS by Comerón et al. (2015), with a poor spatial resolution. In this study, it was proposed that the old thick disc of ESO 533-4 was born already dynamically hot in a turbulent disc or formed from dynamical heating.

Spatially resolved maps of the stellar and gas kinematics with a better resolution were later achieved by Comerón et al. (2019) using MUSE (Multi-Unit Spectroscopic Explorer) for eight late-type field edge-on star-forming disc galaxies. In this study, including five galaxies with a distinct thick disc in the observed region, the accretion of stars from satellite galaxies was disfavored as the main formation mechanism of thick discs. Rautio et al. (2022) took a closer look on the gas content for these five galaxies, where vertical gas velocity gradients or asymmetries in the gas kinematics point to gas accretion (see Sect. 2 for more details). Later on, Martig et al. (2021), Scott et al. (2021), and Sattler et al. (2023) studied the stellar populations of the spiral galaxies NGC 5746, UGC 10738 and NGC 3501. The study of the massive disc galaxy NGC 5746 (Martig et al. 2021) supported the idea

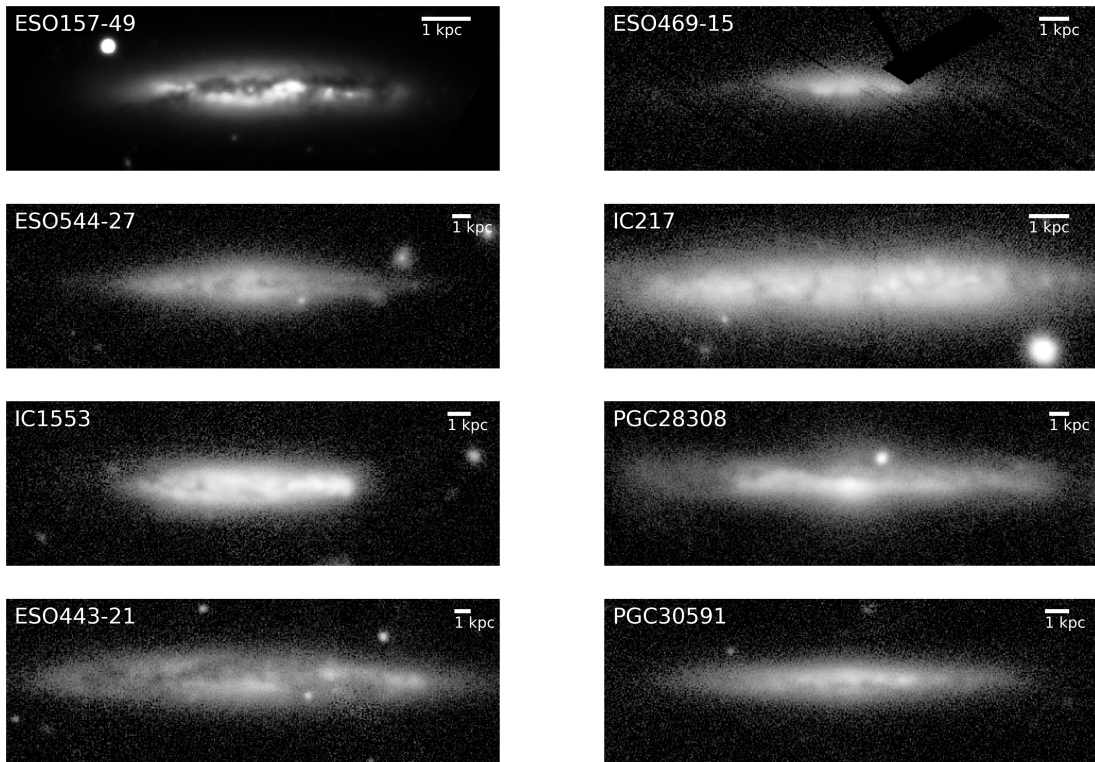


Fig. 1: g -band images of the full sample. The image of ESO 157-49 is taken from the Dark Energy Survey DR2 (Morganson et al. 2018; Abbott et al. 2021), while the other images are from Pan-STARRS1 (Chambers et al. 2016; Magnier et al. 2020a; Waters et al. 2020; Magnier et al. 2020c,b; Flewelling et al. 2020).

(previously proposed by Pinna et al. 2019a,b) that the thick disc might be born already thick in an early phase of evolution, with an additional large fraction of stars (around 30 %) accreted to the thick disc during a merger event around 8 Gyr ago. For NGC 3501, a star-forming galaxy with apparently no morphological distinct thick and thin discs in the observed region, Sattler et al. (2023) found hints of the recent birth and current “inside-out” growth of a thin disc, embedded in a pre-existing thicker disc.

With this paper, we want to extend the knowledge on thin and thick disc formation in spiral galaxies by analyzing in great detail the stellar populations of the eight late-type galaxies for which the kinematics were published by Comerón et al. (2019). The paper is structured as follows: first, we give an overview of the sample in Sect. 2, followed by a description of the observations and data reduction in Sect. 3. Next, the different analytical steps are explained in Sect. 4. The results are presented in Sect. 5 and discussed in Sect. 6. The conclusions are then given in Sect. 7.

2. The sample

The sample consists of the eight edge-on disc galaxies presented in Comerón et al. (2019), who later released their reduced data cubes (see Sect. 3). We show g -band images of the target galaxies in Fig. 1, whereas relevant properties of the sample are indicated in Tab. 1. Galaxies in the sample have morphological types from Sb to Irr (González-Díaz et al. 2024) and masses between 4×10^9 and $6 \times 10^{10} M_{\odot}$ (Muñoz-Mateos et al. 2015).

2.1. Surface brightness profiles

The vertical and radial surface brightness profiles of these galaxies were previously analyzed by Comerón et al. (2018) using Spitzer

S^4G (Sheth et al. 2010) images. For each galaxy, they performed fits on the vertical surface-brightness profiles using the solution of the hydrostatic equilibrium equation under the assumption of two vertically isothermal components (thin and thick disc). Furthermore, central mass concentrations (CMCs) were identified in ESO 157-49, IC 1553, PGC 28308 and ESO 443-21. These can be classical bulges, or boxy/peanut/X-shaped features. In all cases, they were assumed to have a spherical shape and were fitted with a Sérsic function. To fit surface brightness profiles of galaxies hosting this CMC, Comerón et al. (2018) used three components (CMC, thin and thick discs). Based on those fits, they separated their sample of 141 edge-on galaxies into two subsets: galaxies having a thin and thick disc (here the vertical profiles of the thin and thick disc dominate over different heights) and galaxies that do not show two morphologically distinct discs (here the fitted vertical profile of only one component dominates over all heights). Using this definition of the two subsets, the galaxies ESO 157-49, ESO 469-15, ESO 544-27, IC 217 and IC 1553 show two distinct thick and thin disc components that dominate over different heights. For this subsample, we used in the rest of the paper a geometric definition of the thick and thin discs, based on this morphological decomposition where the thick disc starts to dominate over the thin disc at a distance from the midplane equal to z_{c1} (Tab. 1). For ESO 443-21 and PGC 30591, the thick disc component dominates the light along all heights, which is why they were classified by Comerón et al. (2018) as galaxies not showing two distinct disc components. The last galaxy PGC 28308 was found to have distinct and well-defined thin and thick discs. However the thin disc dominates the vertical surface brightness profile at all heights. Because of this, we assign here PGC 28308 to the sub-sample of galaxies that do not have two distinct stellar discs.

Table 1: Properties of the sample galaxies.

Galaxy name	Hubble type ⁽¹⁾	d ⁽²⁾ [Mpc]	$\log(M_*)$ ⁽³⁾ [M_\odot]	r_{25} ⁽⁴⁾ ["]	v_c ⁽⁵⁾ [km s^{-1}]	Discs ⁽⁶⁾	z_{c1} ⁽⁷⁾ ["]	M_t ⁽⁸⁾ [$10^9 M_\odot$]	M_T ⁽⁹⁾ [$10^9 M_\odot$]	SFR ⁽¹⁰⁾ [M_\odot/yr]
ESO 157-49	Sc	17.3	9.81	52.1	107	t + T	6.1	2.54	1.21	0.19
ESO 469-15	Sb	28.3	9.58	55.9	83	t + T	4.8	2.82	1.94	0.20
ESO 544-27	Sb	45.9	9.84	46.5	129	t + T	4.0	7.56	3.57	0.13
IC 217	Scd	21.1	9.75	59.9	115	t + T	5.4	2.46	1.72	0.25
IC 1553	Irr	36.5	9.90	40.5	142	t + T	5.0	8.63	4.00	0.96
PGC 28308	Scd	43.1	10.81	59.9	130	t*+ T	-	-	-	(0.51)
ESO 443-21	Scd	52.2	10.34	36.9	196	-	-	-	-	(2.40)
PGC 30591	Sd	35.5	10.21	45.4	97	-	-	-	-	(0.29)

Notes: (1) Morphological types from [González-Díaz et al. \(2024\)](#); (2) Distances (d) from [Tully et al. \(2008, 2016\)](#); (3) Stellar masses (M_*) from [Muñoz-Mateos et al. \(2015\)](#); (4) Radii (r_{25}) from HyperLeda ([Makarov et al. 2014](#)); (5) Circular velocities (v_c) from [Comerón et al. \(2019\)](#); (6) Disc structures (t: thin disc, T: thick disc, *: thin disc dominates at all heights) from [Comerón et al. \(2018\)](#); (7) Distance from the midplane beyond which the thick disc is dominant (z_{c1}); (8) and (9) Masses of the thin (M_t) and thick discs (M_T); (10) Star formation rates (SFR) from [Rautio et al. \(2022, 2024\)](#), where values in brackets have high uncertainties.

2.2. Kinematic studies

[Comerón et al. \(2019\)](#) extracted and analyzed the kinematics of the stellar and gas content from the same data used here (Sect. 3). They obtained spatially resolved maps of stellar velocities and velocity dispersions, together with gas velocities for these galaxies. From the gas velocity maps, they extracted the midplane gas rotation curves and fitted these to estimate the circular velocities which are listed in Tab. 1. On average, they detected lower velocity dispersions for the thin disc (with values lower than 20 km s^{-1}) than for the thick disc ($40\text{-}60 \text{ km s}^{-1}$). Also, the galaxies without distinct thick and thin disc components show this pattern of lower velocity dispersion for the midplane compared to regions at larger heights. This pattern is a consequence of asymmetric drift of the gas and found in many observed galaxies, as pointed out in Sect. 1. For PGC 28308, the highest velocity dispersion of around 70 km s^{-1} is present in a spheroidal central structure, that results from a central mass concentration hosting 10 % of PGC 28308’s baryonic mass ([Comerón et al. 2019](#)).

2.3. Gaseous properties

Using the same MUSE data analyzed by [Comerón et al. \(2019\)](#) and in this paper, together with deep narrow-band $H\alpha$ images, [Rautio et al. \(2022, 2024\)](#) analyzed the ionized-gas content for the full sample of eight galaxies. They found significant complexity in the extraplanar diffuse ionized gas (eDIG) and $H\text{II}$ regions. Moreover, they calculated the star formation rates (SFR) for those galaxies, and divided their subsample into star-forming and green valley galaxies. The more quiescent galaxy ESO 544-27 has a $\text{SFR} = 0.13 M_\odot/\text{yr}$, placing it into the green valley, while also PGC 28308 ($\text{SFR} = 0.51 M_\odot/\text{yr}$) and PGC 30591 ($\text{SFR} = 0.29 M_\odot/\text{yr}$) fall within this regime. The other galaxies, ESO 157-49 ($\text{SFR} = 0.19 M_\odot/\text{yr}$), ESO 469-15 ($\text{SFR} = 0.20 M_\odot/\text{yr}$) and IC 217 ($\text{SFR} = 0.25 M_\odot/\text{yr}$) lay in the star-forming regime, very close to the line separating it from the green valley. IC 1553 ($\text{SFR} = 0.96 M_\odot/\text{yr}$) and ESO 443-21 ($\text{SFR} = 2.40 M_\odot/\text{yr}$) have the highest SFR of the sample and seem to fall well within the star-forming regime. However, the SFR measurements for ESO 443-21, PGC 28308 and PGC 30591 have high uncertainties due to their incomplete spatial coverage in the MUSE field-of-view and should be handled with caution. Moreover, [Rautio et al.](#)

(2022) found signs of gas accretion in several galaxies of the sample. Furthermore using eDIG kinematics, Baldwin-Phillips-Terlevich (BPT, [Baldwin et al. 1981](#)) diagrams and $H\alpha$ intensity maps [Rautio et al. \(2022, 2024\)](#) discussed the ionization sources of the galaxies. While the ionization by in-situ evolved stars is insignificant for most of the galaxies in our sample, it may be able to explain enhanced high-ionization lines in the eDIG of the green valley galaxy ESO 544-27. Another study by [González-Díaz et al. \(2024\)](#) analyzed the gas content in the halos of this same sample of eight galaxies using the same MUSE data by [Comerón et al. \(2019\)](#). They suggested the halo gas emission in general originates from feedback-induced shocks from strong star formation in the disc and found hints of an “intricate dynamical heating structure” at large distances from the midplane.

The modeling of the kinematics of the ionized gas by [Rautio et al. \(2022\)](#) in ESO 157-49 shows strong evidence for gas accretion, while also the highest $H\alpha$ intensity is observed on the western side of the thin disc approximately 20 arcsec from the center. Asymmetries in the eDIG of the halos were also observed by [González-Díaz et al. \(2024\)](#). Since ESO 157-49 has a nearby companion dwarf (ESO 157-48) with a projected distance of 14.2 kpc, this companion might be a gas accretion source. Further studies of ESO 157-49 ([Keeney et al. 2013](#)) showed signs of a galactic fountain of recycled gas in the kinematics of major axis clouds, while clouds along the minor axes were constrained to be outflowing gas. Outflows for ESO 157-49 were also suggested in [López-Cobá et al. \(2020\)](#).

ESO 469-15 contains discrete extraplanar $H\text{II}$ regions at larger heights (3 kpc) above the midplane (in the region dominated by the thick disc) and also more outwards (8 kpc) in the radial direction from the center ([Rautio et al. 2022](#)). These $H\text{II}$ regions, with lower rotation velocities and larger velocity dispersions than the ones near the midplane, may cause a more enhanced vertical gradient in the gas rotation velocity than the diffuse gas itself, pointing to a different origin for those $H\text{II}$ regions from the eDIG. The galaxy with the lowest star formation rate, ESO 544-27 shows an asymmetric vertical gas-velocity gradient, on the southwestern side of the midplane, which can be explained by gas accretion ([Rautio et al. 2022](#)). However, [González-Díaz et al. \(2024\)](#) find a homogeneous distribution of $H\text{II}$ regions in the halo and no strong asymmetries along the major axis. Besides being the most quiescent galaxy, it was also suggested by [Rautio et al. \(2022\)](#) that

ESO 544-27 has older stellar populations than the other galaxies. IC 217 shows an asymmetric eDIG morphology with very pronounced filaments on the southwestern half and minimal emission on the northeastern one. A vertical gas velocity gradient could not be confirmed with the MUSE data in Rautio et al. (2022), since the region with high $H\alpha$ emission is not fully covered by the data. However, asymmetries in the gas hint at gas accretion.

The most strongly star-forming galaxy, the irregular galaxy IC 1553 (Tab. 1), shows a rich and asymmetric eDIG morphology with numerous filaments, an extraplanar $H\text{II}$ region on the western side and very pronounced eDIG emission on the southern half (Rautio et al. 2022). This galaxy shows a negative vertical gas velocity gradient on the side with high $H\alpha$ emission, suggesting an accretion origin for the gas. This same high emission region coincides with a conical-shaped structure above and below the midplane in various emission line ratio maps (see also González-Díaz et al. 2024).

Tully et al. (2009) found that the $H\text{I}$ line profile for PGC 28308 is antisymmetric, which could indicate disturbed outskirts. Moreover, concentrated eDIG above the center of this galaxy could hint at ionization by outflow driven shocks Rautio et al. (2024). Also, PGC 28308 forms a pair with the galaxy MCG-02-25-019 in the HIPASS catalog (Meyer et al. 2004) that has a projected distance of 59 kpc (Rautio et al. 2022).

2.4. More studies

In a study by Schwarzkopf & Dettmar (2000), edge-on disc galaxies were divided into non-interacting and interacting/minor-merging candidates. There, we only find one of our eight sample galaxies, ESO 443-21, which falls into the interacting/minor-merging candidate sample. In Zaragoza-Cardiel et al. (2020), stellar population properties were measured over several 500 pc sized regions across the whole galaxy discs of ESO 443-21, IC 217, IC 1553, PGC 28308 and PGC 30591 and the SFRs for “recent” (0.01 Gyr) and “past” (0.57 Gyr) age bins were derived. For ESO 443-21, most regions have a strong recent star formation, while for PGC 28308, PGC 30591 and IC 217 the SFR was higher in the past. In IC 1553, most regions show stronger past star formation, but there is still a significant amount of regions with more star formation in recent ages. Lastly, Somawanshi et al. (2024) performed a stellar population analysis, following the same approach as in Pinna et al. (2019b,a) and Sattler et al. (2023), of the galaxy ESO 544-27. They found that this galaxy is overall old (> 9 Gyr) and metal-rich, with no clear differences between the thick and thin discs. However, a dichotomy in $[\alpha/\text{Fe}]$ is found with a low- $[\alpha/\text{Fe}]$ thin disc and high- $[\alpha/\text{Fe}]$ outer thick disc. They also detected a young (< 2 Gyr) metal-rich stellar population most present in the outer thick disc (Fig. 9 in Somawanshi et al. 2024). Therefore, they propose that the thin and thick disc of ESO 544-27 formed in-situ. During the evolution, the star formation was nearly quenched between 2 to 8 Gyr and reignited around 1 Gyr ago in the thick disc, probably by a wet merger event, and very recently (~ 600 Myr ago) in the thin disc.

3. Observations and data reduction

We used the archival data published by Comerón et al. (2019). Observations were taken using MUSE (Bacon et al. 2010) at the Unit Telescope 4 of the VLT (Very Large Telescope) in Paranal. MUSE is a panoramic integral-field spectrograph with a field-of-view of $1' \times 1'$ in the Wide-Field Mode (WFM) and a pixel size of $0.2'' \times 0.2''$. It can observe in a wavelength range of

4750 to 9300 Å with a spectral resolution $R = 2000$ at the blue end and $R = 4000$ at the red end (Bacon et al. 2017).

The observations correspond to the ESO programs 097.B-0041 and 096.B-0054¹ (P.I. Sebastian Comerón) released on 25th September 2019² (Comerón et al. 2019) and were carried out between December 2015 and August 2016. For seven out of the eight galaxies, four on-target exposures of 2624 s each were executed, but only three on-target exposures of the same time were taken for IC 217, resulting in a lower total exposure time for this galaxy. The single exposures were all centered at the same position with a rotation of 90° between each other.

For the data reduction, Comerón et al. (2019) used the MUSE pipeline version 1.6.2 (Weilbacher et al. 2012) in the REFLEX environment (Freudling et al. 2013). The different exposures of each galaxy were combined to get a single data cube for each galaxy. Off-target sky frames with an exposure time of 240 s were also taken, but they were not used in the later data reduction because of large sky variations between on- and off-target exposures coming from the relatively long on-target exposures. Nevertheless, Comerón et al. (2019) accounted for the sky by modeling it from regions in the on-target exposures, that have a larger distance from the galaxy midplane. Following that, the combined cubes were cleaned from the sky residuals with ZAP version 2.1 (Soto et al. 2016).

4. Methods

We describe here the methods that we applied to the data. While this paper focuses on the stellar populations of our galaxy sample, whose analysis is described in Sect. 4.3, some previous steps were necessary to prepare the data and are described in Sect. 4.2. The stellar population models used in all these steps are described in Sect. 4.1.

4.1. Stellar population models

To fit the spectra of the MUSE data cubes as described in the next sections, a spectral library of stellar models needs to be used. We used the Vazdekis et al. (2015) MILES SSP (Single-Stellar Population) models in this analysis. These models have a spectral resolution of 2.51 Å (Falcón-Barroso et al. 2011) and cover the wavelength range from 3540 to 7410 Å. After testing different subsets of models (see App. B), we decided to use the full range of MILES SSP models including:

- 12 metallicity $[\text{M}/\text{H}]$ values from -2.27 dex up to 0.40 dex
- 53 age values from 0.03 to 14 Gyr
- 2 $[\alpha/\text{Fe}]$ values: 0.0 dex (solar abundance) and 0.4 dex (super-solar abundance)

This adds up to 1272 models in total, where each model is associated to a combination of age, metallicity and $[\alpha/\text{Fe}]$ -abundance. As we are focusing around the Mgb region, we use $[\text{Mg}/\text{Fe}]$ as tracer of $[\alpha/\text{Fe}]$.

¹ https://archive.eso.org/scienceportal/home?data_collection=096.B-0054

² <https://www.eso.org/sci/publications/announcements/sciann17233.html>

4.2. Data cube preparation

4.2.1. Voronoi binning

As the first step, we cut the data cubes of each galaxy to a specific spatial range to exclude bad pixels at the top and bottom edges of the pointings. Also, we masked prominent foreground objects that would influence further analysis and results.

After that, we binned each data cube with the Voronoi binning (VORBIN) method by Cappellari & Copin (2003). This method combines different pixels of given integral-field spectroscopy data with an adaptive spatial binning to reach a target SNR (Signal-to-Noise Ratio) per Voronoi bin while preserving the maximum possible spatial resolution of the data. We performed the VORBIN method on the whole sample using a SNR-threshold of 1, meaning that only pixels with a larger SNR than the SNR-threshold are used for the combination into the Voronoi bin. We chose this relatively low SNR-threshold to cover the fainter thick-disc regions. However, since for IC 217 the exposure time was relatively short (see Sect. 3), the thick disc of this galaxy is not well covered by our Voronoi bins.

We first tested a target-SNR = 40, but stellar populations of ESO 469-15 and IC 1553 showed very large uncertainties (as calculated according to Sect. 4.3.3), especially in age and metallicity. We decided to increase the target SNR to 60 for all galaxies, after proving that the uncertainties in the stellar populations scaled down. Also, the emission line fits (described in Sect. 4.2.2) of ESO 469-15 improved with the higher target-SNR Voronoi binning. For IC 1553, the target-SNR = 60 Voronoi binning did not improve significantly the quality of the fits and the uncertainties, so we increased the target SNR to 100 for this galaxy. A summary of the used target-SNR for each galaxy can be found in Tab. 2.

Lastly, the spectra of each bin were cut to the wavelength range between 4750 to 5500 Å, to avoid regions at longer wavelengths where the sky subtraction might have left residuals, and to also exclude regions that are not relevant for the analysis here as they do not contain α -element or age-sensitive features.

4.2.2. Gas emission line fitting

We fitted the gas emission to subtract it from the observed spectrum. We needed to achieve an emission-cleaned spectrum to fit the stellar populations without having to mask the regions of important age-sensitive features, like the $H\beta$ λ 4861 absorption.

For the fitting of the emission lines, we first tested GANDALF written by Sarzi et al. (2006) and previously used by Sattler et al. (2023). But when looking at the fits, we noticed that GANDALF produced large residuals with wiggles for very strong emission lines, for $H\beta$ λ 4861 and $[O\ III]\lambda$ 5007, especially in ESO 157-49, ESO 443-21, ESO 469-15, IC 217, IC 1553 and PGC 30591. This resulted in many badly fitted Voronoi bins. We then tested different setups for GANDALF:

- Fit kinematics of all lines free
- Fit kinematics of $[O\ III]\lambda$ 4959,5007 & $[N\ I]\lambda$ 5198 tied to $H\beta$
- Fit kinematics of $[N\ I]\lambda$ 5198 & $[O\ III]\lambda$ 4959 tied to $[O\ III]\lambda$ 5007
- Fit kinematics of $[O\ III]\lambda$ 4959 tied to $[O\ III]\lambda$ 5007 & fit $[N\ I]\lambda$ 5198 free

but none of them really improved the fitting of the emission lines.

Further, we tested to fit the emission lines with PPF (Cappellari 2017, 2022) using one gas component. Using the variable LSF of MUSE, the stellar continuum is fitted with combinations of SSP

models, while Gaussian templates are added to this continuum by PPF to fit the emission lines. For each of the 4 emission lines $H\beta$ λ 4861, $[O\ III]\lambda$ 4959,5007 and $[N\ I]\lambda$ 5198, a separate Gaussian template was created and fitted. Those templates were fixed to the same kinematics but allowed to vary in amplitude. We obtained the flux, velocity V and velocity dispersion σ of the ionized gas. Using PPF, the galaxies showed better fitted Voronoi bins than before. Still, ESO 157-49, ESO 469-15, IC 217, ESO 443-21 and PGC 30591 showed large residual in the regions of $[O\ III]\lambda$ 4959,5007 emission. Further, for IC 1553 all the emission lines were fitted poorly for many Voronoi bins, since the lines were asymmetric and had too much deviation from a true Gaussian shape, such that only one Gaussian template did not fit the lines well enough. Because of that, we tested for this galaxy the use of two gas components, i.e. two Gaussian templates with different kinematics, per emission line. However, this approach still gave large residuals of the fits. Only ESO 544-27 and PGC 28308 showed good fits without any larger residuals for all emission lines.

After fitting the gas emission lines, the “gas best-fit” spectra (consisting of the best-fitting Gaussian gas templates) were subtracted from the observed galaxy spectra for each Voronoi bin and emission-cleaned spectra were obtained for all galaxies. In general, the gas emission was quite high for some galaxies and had fluxes up to 20 times higher than the stellar continuum. Because of this, the subtraction of the “gas best-fit” spectra left large wiggles in the emission cleaned spectrum, even if the gas emission lines themselves showed good fits (similar to what was reported by Domínguez-Gómez et al. 2023). This is because the residuals of the gas emission were larger than the noise of the spectra. For this reason the emission-cleaned stellar spectra of ESO 157-49, ESO 443-21, ESO 469-15, IC 217, IC 1553 and PGC 30591 showed large residual wiggles, especially in the $[O\ III]\lambda$ 4959,5007 emission regions, and for IC 1553 also the $H\beta$ λ 4861 emission region. Our strategy to deal with these wiggles will be explained in Sect. 4.3.1.

4.2.3. Extinction correction

Because late-type galaxies usually contain large amounts of gas and dust, we corrected the galaxy spectra for interstellar extinction before fitting for stellar populations. Therefore, we followed the same procedure used in Sattler et al. (2023), where we first fitted each Voronoi bin spectrum for extinction with PPF by using the built-in reddening parameter. We then removed the extinction from the spectra using version 0.4.6 of the EXTINCTION³ package. Following Emsellem et al. (2022), we also corrected all spectra for Galactic extinction of the Milky Way by division with the Cardelli et al. (1989) extinction law.

4.3. Stellar population analysis

4.3.1. Stellar population fitting

To extract the stellar populations (age, metallicity and $[Mg/Fe]$ -abundance) from the extinction corrected spectra, we fitted those with PPF including a regularization (Cappellari 2017). This regularization leads to smoother weight distribution on the different SSPs and thus smoother stellar population solutions. Regularization helps to avoid spurious stellar population solutions that are unstable against changes in the fitting process. A good choice of the regularization parameter is necessary to avoid smoothing to the

³ <https://extinction.readthedocs.io/en/latest/>

Table 2: Summary of settings for the sample.

Galaxy	SNR ⁽¹⁾	# bins ⁽²⁾	masked for pop ⁽³⁾
ESO 157-49	60	1422	[O III]
ESO 469-15	60	559	[O III]
ESO 544-27	60	476	-
IC 217	60	252	[O III]
IC 1553	100	387	H β + [O III] + [N I]
PGC 28308	60	188	-
ESO 443-21	60	268	[O III]
PGC 30591	60	176	[O III]

Notes: (1) Target-SNR for the Voronoi bins; (2) Number of Voronoi bins; (3) Emission line regions that got masked for the stellar population fitting.

extent such that minor stellar population components disappear in the distributions of age, metallicity or [Mg/Fe]-abundance. To find the maximum value of regularization, we followed the approach given in the `PPXF` code itself (Cappellari 2017, 2022), also used by Pinna et al. (2019b,a), Boecker et al. (2020), and Sattler et al. (2023). We applied this approach to one central Voronoi bin of each galaxy, following the steps below:

1. A fit was performed with noise = 1 and regularization = 0, so that $\chi^2 = N_{\text{goodpix}}$
2. The noise was re-scaled to $\sqrt{\frac{\chi^2}{N_{\text{goodpix}}}}$, while the `PPXF` fit was iteratively repeated increasing regularization, until $\Delta\chi^2 \approx \sqrt{2N_{\text{goodpix}}}$

This final value of regularization was the maximum regularization parameter. A variety of values lower than the upper limit still give results that are consistent with the data. After testing different values of regularization (see App. B), we decided to use a value of 1 for all galaxies, as it applied some smoothing but allowed the identification of features in the star formation histories.

To recover those spatial bins with large residuals resulting from the emission line subtraction, we masked in the emission-cleaned spectra of ESO 157-49, ESO 443-21, ESO 469-15, IC 217 and PGC 30591 the regions of [O III] $\lambda\lambda 4959, 5007$ emission with a window of 400 km s^{-1} for the stellar population fitting. For IC 1553, we used the original Voronoi binned spectra for the fitting and masked the region of H β $\lambda 4861$, [O III] $\lambda\lambda 4959, 5007$ and [N I] $\lambda 5198$ emission. A summary of the setup can be seen in Tab. 2.

We fitted all galaxies for light- and mass-weighted stellar population parameters. The chosen SSP models (Sect. 4.1) are normalized to have $1 M_{\odot}$ at birth. So, any further normalization was not necessary to extract mass-weighted stellar population parameters. We normalized the SSP models by their mean flux to obtain light-weighted results. Also, we applied a multiplicative polynomial of 8th degree and no additive polynomials during the fitting process and discarded all Voronoi bins that were ill-fitted (the shape of the spectrum was not followed or large residuals were present).

4.3.2. Star formation histories

For the extraction of the star formation histories, normalized by the mass of the covered region of the galaxy, we first calculated

the mass-to-light ratio for each Voronoi bin by combining the mass-to-light ratios of the MILES SSP models (Vazdekis et al. 2015) with the mass-weighted stellar population results. To calculate the mass of each Voronoi bin as in Pinna et al. (2019b) and Sattler et al. (2023), we additionally used g -band images (see Fig. 1) from Pan-STARRS1⁴ (Chambers et al. 2016; Magnier et al. 2020a; Waters et al. 2020; Magnier et al. 2020c,b; Flewelling et al. 2020) for ESO 443-21, ESO 469-15, ESO 544-27, IC 217, IC 1553, PGC 28308 and PGC 30591. For ESO 157-49, not part of the Pan-STARRS1 sample, we used a g -band image from the Dark Energy Survey DR2⁵ (Morganson et al. 2018; Abbott et al. 2021). Then, we converted the g -band magnitudes into V -band magnitudes, following Pinna et al. (2019b). Taking into account the distances to the galaxies, we calculated the total mass in each MUSE pixel. These masses per pixel were then multiplied by the number of pixels for each Voronoi bin, to get the mass of the entire Voronoi bin.

To obtain the star formation histories of the different disc components, we defined the regions of the thin and thick discs using the heights above and below which the thick disc dominates z_{c1} (see Tab. 1). For galaxies with CMCs (see Sect. 2), although these CMC do not dominate at any time the vertical surface brightness profiles, we decided to ignore the central region from the thin discs, to avoid any potential contamination from the CMCs. Therefore, we discarded all Voronoi bins in a central region within r_{CMC} , the scale radius of the Sérsic profile of the CMC (Comerón et al. 2018). However, as the Voronoi bins are already quite large in the central regions, this CMC region is not a perfect circular cut. Since the thin discs of ESO 157-49 and IC 1553 showed in the metallicity maps (presented in Sect. 5.1) a region with a much lower metallicity than other comparable regions in the thin disc, we found it interesting to also extract the star formation histories of these metal-poor regions. The different regions for which we traced the star formation histories are mapped in Fig. 2. To obtain the star formation histories, we summed up the weights from the mass-weighted results for each Voronoi bin belonging to the component, so all the mass fractions corresponding to the same age bin with different metallicities and [Mg/Fe]-abundances. Then, we computed a mass-weighted average of the mass fractions per age for all Voronoi bins normalized by the galaxy mass. As the age resolution changes from 0.01 Gyr up to 0.5 Gyr in the latest 4 Gyrs (after an age of 4 Gyr the resolution stays consistent with 0.5 Gyr), we further summed up the mass fractions of the different age bins to achieve a stable resolution among all ages. This will help to better compare the mass fractions for all the ages with different resolutions.

4.3.3. Monte Carlo simulations

To estimate the uncertainties in the stellar populations and star formation histories, we performed Monte Carlo simulations. Hence, we followed these steps for each Voronoi bin of the galaxies for 1000 realizations:

1. From the stellar population fits with `PPXF`, calculate the wavelength-dependent residuals as the difference between the best-fitted model spectrum and the observed galaxy spectrum

⁴ <https://outerspace.stsci.edu/display/PANSTARRS/Pan-STARRS1+data+archive+home+page>

⁵ <https://www.darkenergysurvey.org/>

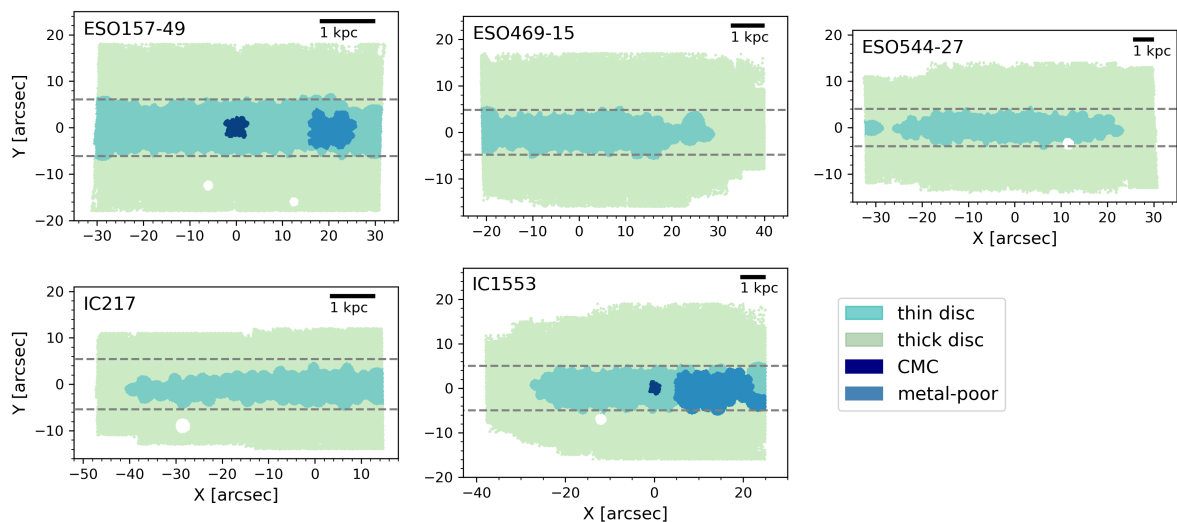


Fig. 2: Component decomposition for the five out of the eight sample galaxies containing distinct thick and thin discs.

Table 3: Average uncertainties for the light-weighted stellar population maps (Fig. 3) calculated as the mean uncertainty of all bins belonging to the corresponding component. The detailed uncertainty maps can be seen in App. D.

Galaxy	Component	ΔAge [Gyr]	$\Delta[\text{M}/\text{H}]$ [dex]	$\Delta[\text{Mg}/\text{Fe}]$ [dex]
ESO 157-49	thin disc	0.30	0.05	0.12
	thick disc	1.23	0.10	0.13
ESO 469-15	thin disc	0.33	0.05	0.12
	thick disc	1.85	0.17	0.19
ESO 544-27	thin disc	0.31	0.05	0.07
	thick disc	1.52	0.11	0.18
IC 217	thin disc	0.30	0.07	0.10
	thick disc	0.93	0.08	0.13
IC 1553	thin disc	0.93	0.24	0.31
	thick disc	3.02	0.48	0.23
PGC 28308	full galaxy	0.32	0.04	0.14
ESO 443-21	full galaxy	0.48	0.07	0.24
PGC 30591	full galaxy	0.30	0.05	0.08

- For each realization, calculate the noise spectrum as a random noise from a Gaussian distribution with a standard deviation equal to the residuals at each wavelength.
- Add this random noise to the observed spectrum, so that a different noise is applied for each realization.
- Fit this new noisy spectrum with `PPXF` for stellar populations using no regularization.

Thereafter, we calculated the uncertainties in age, metallicity and $[\text{Mg}/\text{Fe}]$ -abundance for each Voronoi bin as the standard deviation of the age, metallicity and $[\text{Mg}/\text{Fe}]$ distributions from these 1000 realizations. To obtain the uncertainties of the star formation histories, we computed a separate star formation history for each of the 1000 Monte Carlo realizations and determined the standard deviation from the mean mass fractions for each age.

5. Results

5.1. Mapping stellar populations

In this section, we present the light-weighted stellar population maps (Fig. 3). Mass-weighted results, which were used for the star formation histories, are shown in App. C. Average uncertainties for the light-weighted stellar population maps can be seen in Tab. 3 and maps of the uncertainties for each Voronoi bin can be found in Fig. D.1. As the uncertainties in the stellar populations can be large, especially for IC 1553, we need to be cautious with quantitative analysis based on the absolute values and set the focus on the relative differences between the thin and thick discs.

Taking a look at the light-weighted age maps (Fig. 3, left column), most galaxies with clear distinct thin and thick discs (ESO 157-49, ESO 469-15, ESO 544-27, IC 1553) show on average very young stars (< 2 Gyr) in the thin disc and older stars (in a wide range from 3 to 11 Gyr) in the thick disc region. Thereby, the thick disc of IC 1553 shows the youngest ages staying below 4 Gyr. IC 217, which also has two disc components in the vertical surface brightness profiles, shows no clear differences in thin and thick disc ages, the whole galaxy is rather young with ages below 7 Gyr. For ESO 157-49, the oldest stars with ages around 6 to 8 Gyr are located in the inner transition region between the thick and the thin disc, and might be related to a central component (Sect. 2.1). The boxy shape suggests this might be a boxy bulge. In the thick disc of ESO 544-27 the ages decrease from around 8 Gyr at smaller radii to below 3 Gyr at larger radii, suggesting a thin disc flaring. For IC 1553, a similar behavior is observed in the thick disc region only above the thin disc. Ages decrease towards larger radii (from about 4 Gyr to very recent ages) suggesting a warp.

Galaxies without clear distinct thin and thick discs (PGC 28308, ESO 443-21 and PGC 30591) show in general a similar structure as the rest of the sample with younger stars along the midplane and older stars for regions at larger heights. However, there is some more variance from galaxy to galaxy. For PGC 28308 in particular, the oldest stars (as old as 11 Gyr) are located at the largest distances from the midplane in a spheroidal shape.

In the light-weighted metallicity maps (Fig. 3, middle column), most galaxies with clear distinct thin and thick discs

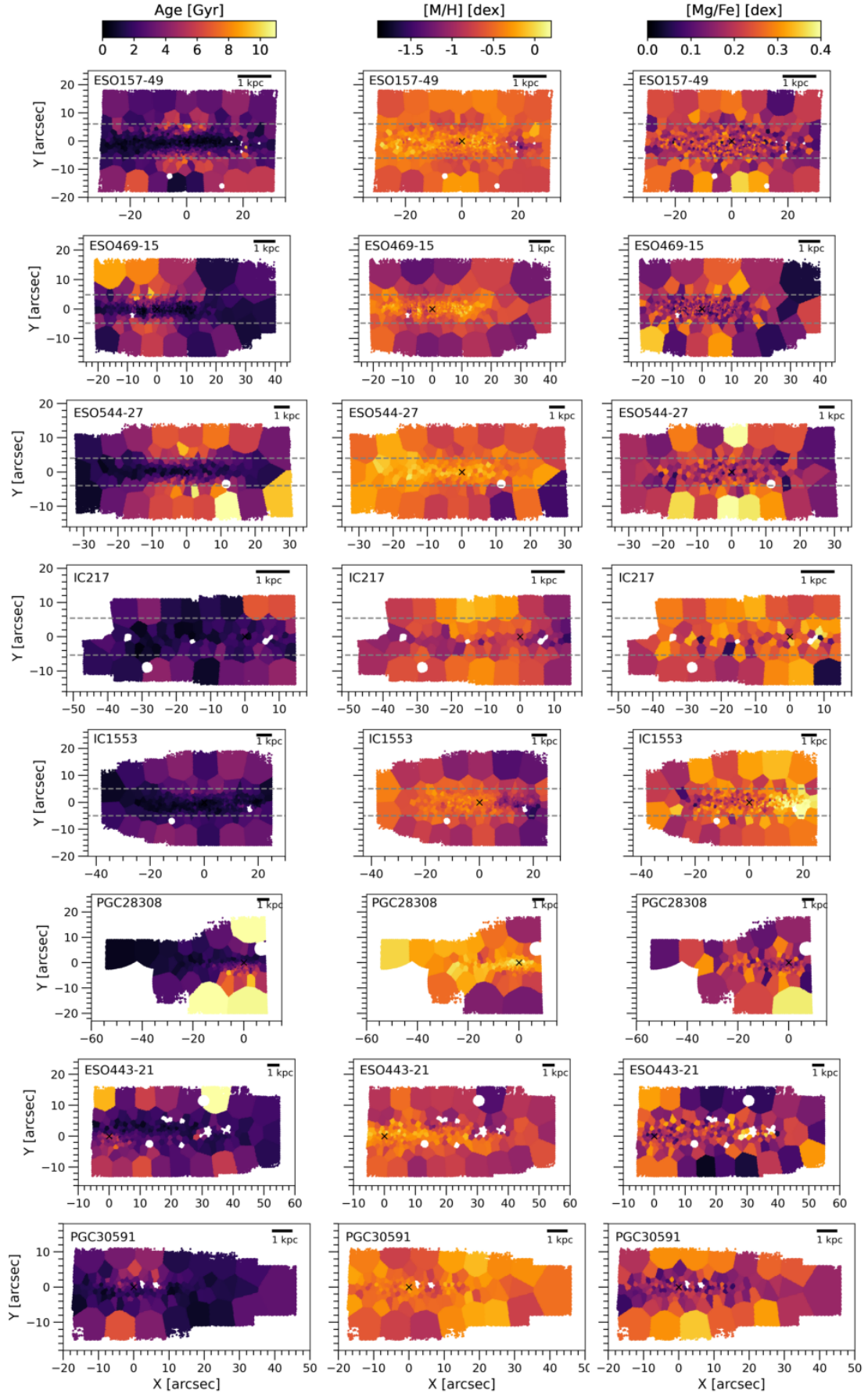


Fig. 3: Light-weighted age (left), metallicity (middle) and [Mg/Fe]-abundance (right) maps for the full sample. For the galaxies with distinct morphological thick and thin discs, grey dashed lines mark the regions above and below which the thick disc dominates the vertical surface-brightness profiles.

Table 4: Mass fractions of the different regions.

Galaxy	thick disc	thin disc	metal-poor
ESO 157-49	0.22	0.76	0.05
ESO 469-15	0.23	0.77	-
ESO 544-27	0.39	0.61	-
IC 217	0.33	0.67	-
IC 1553	0.22	0.77	0.19

(ESO 157-49, ESO 469-15, ESO 544-27 and IC 1553) show higher metallicities (nearly solar) in the thin discs and lower sub-solar metallicities in the thick discs. Besides, ESO 157-49 and IC 1553 show a region with very low metallicity (even lower than the average of the thick disc) in their thin discs around 20 arcsec (for ESO 157-49) and 5-25 arcsec (for IC 1553) to the right from the galaxy center. In contrast to the other galaxies with distinct thin and thick discs, interestingly, IC 217's thin disc is slightly metal-poorer than the thick disc. Having no distinct thin and thick disc components, the galaxies PGC 28308 and ESO 443-21 follow the same trend with higher (nearly solar) metallicities in the central midplane regions and lower clearly sub-solar metallicities for regions at larger heights. For PGC 30591, there are no clear metallicity differences with sub-solar values all over the disc.

The light-weighted [Mg/Fe] maps are shown in the right column of Fig. 3. ESO 157-49, ESO 469-15, ESO 544-27, IC 1553 and PGC 30591 show in general lower [Mg/Fe]-abundances in the thin discs or midplane regions and higher abundances for regions at larger heights. In IC 1553, the most [Mg/Fe]-rich region is located in the thin disc and spatially matches the most metal-poor region that we have mentioned in the previous paragraph. However, all the [Mg/Fe] distributions are quite noisy and due to the uncertainties being larger than 0.1 dex for most of the galaxies, part of these differences are not significant. For the remaining galaxies (IC 217, PGC 28308 and ESO 443-21) no signs of structures in the [Mg/Fe] distributions can be identified.

5.2. Star formation histories

The star formation histories for the whole stellar discs and the different components as defined in Sect. 4.3.2 and Fig. 2 (thin disc, thick disc, and metal-poor region) of the sample galaxies are presented in Fig. 4. In these plots, the mass fractions for each of the components are shown as functions of age together with the uncertainties (shaded region). It is important to recall that these star formation histories were extracted from the mass-weighted results (App. C), where average ages are older than the ones shown in Fig. 3. The fractional contributions of thin and thick discs and metal-poor regions to the stellar mass of the analyzed region of the galaxy are contained in Tab. 4. There, the mass fractions given for the combined thin disc and thick disc of ESO 157-49 and IC 1553 are smaller than 100 %, because the central regions including the CMCs were excluded from the thin disc component. The metal-poor regions mass is however included in the mass fraction of the thin disc.

In the star formation histories of the full galaxies (Fig. 4, left column), star formation started at very early times with a very large amount of stars formed at old ages for all galaxies. After that, the star formation dropped around 11 Gyr and increased

again at intermediate ages (about 8-9 Gyr ago) for ESO147-49, ESO 544-27 and IC 1553. This higher star formation forms a plateau emerging between 4 to 9 Gyr for IC 1553. On the other hand, ESO 469-15, IC 217, PGC 28308, ESO 443-21 and PGC 30591 have a flatter slope with roughly constant star formation at intermediate ages. At the youngest ages, all galaxies show a final burst at more recent times.

If we look at the star formation histories of the thick discs (Fig. 4, middle column), fewer stars are formed at the oldest ages compared to the whole galaxies. At intermediate ages (around 8 Gyr), the thick discs of ESO 157-49, ESO 469-15 and ESO 544-27 show respectively a medium, a mild and a strong increase in star formation. Most of the mass in the thick disc was formed during this star-forming episode in ESO 157-49 and ESO 544-27, while ESO 469-15 formed its thick disc more steadily. IC 217 and IC 1553 also show a relatively steady thick disc star formation history without any rapid increase. Afterwards, ESO 157-49 and ESO 469-15 show a continuous decrease in star formation with nearly no stars formed at recent times. The thick discs of ESO 544-27, IC 217 and IC 1553 display a late star-forming episode at recent times. However, mass fractions have large uncertainties for these young ages (shaded regions).

In the thin discs (Fig. 4, right column), mass weights are in general distributed mostly in the very old and young populations. However, it should be taken into account that the separation of thin and thick discs is not a straight forward process and the thin disc spectra contain contamination of thick disc light. For ESO 157-49, ESO 469-15 and ESO 544-27 the increase in star formation around 8 Gyr in the thin discs is not as pronounced as in the thick discs, while for IC 1553 we see a prominent plateau along intermediate ages. The thin disc of IC 217 shows a continuous decrease in star formation from oldest ages to around 4 Gyr and seems to get almost totally quenched along intermediate ages. At youngest ages, all galaxies show a final starburst, with a different time scale and strength for different galaxies. Although some stars were also formed at thick disc heights during these final starbursts, it is much more pronounced in the thin discs compared to the thick discs.

For two galaxies, we extracted the star formation history of the metal-poor regions in the thin disc (Sect. 4.3.2). These are shown in the lower right corner of Fig. 4. In ESO 157-49, the final starburst at the youngest ages contributed more stellar mass compared to the peak around 8 Gyr. For the metal-poor component in IC 1553, two separate peaks emerge between 4 to 9 Gyr showing combined the highest amount of star formation compared to other ages.

Even with this target-SNR = 60 and 100 Voronoi binning, uncertainties in the mass fractions are quite large for the thick discs ($\pm 1\%$ of the galaxy mass) and especially for the oldest ages (up to $\pm 2\%$ of the galaxy mass). For the thin discs, these are much lower on average ($\pm 0.2\%$ of the galaxy mass) and similar to the ones for the full galaxies, while the uncertainties for the metal-poor regions vary between $\pm 0.1\%$ and $\pm 0.2\%$ of the galaxy mass.

For nearly all galaxies (except ESO 157-49 and IC 1553), the highest peak in the global-galaxy star formation is located at the oldest ages with a decrease afterwards, suggesting very intense star formation at the beginning of galaxy evolution. However, this large mass fraction at the oldest ages might be due to a well-known and tested bias from PPF towards very old stellar populations (Pinna et al. 2019b; Wang et al. 2023). It should be pointed out, that we also analyzed the chemical evolution as from the distributions of metallicity and [Mg/Fe]-abundances associated to different ages, following Sattler et al. (2023).

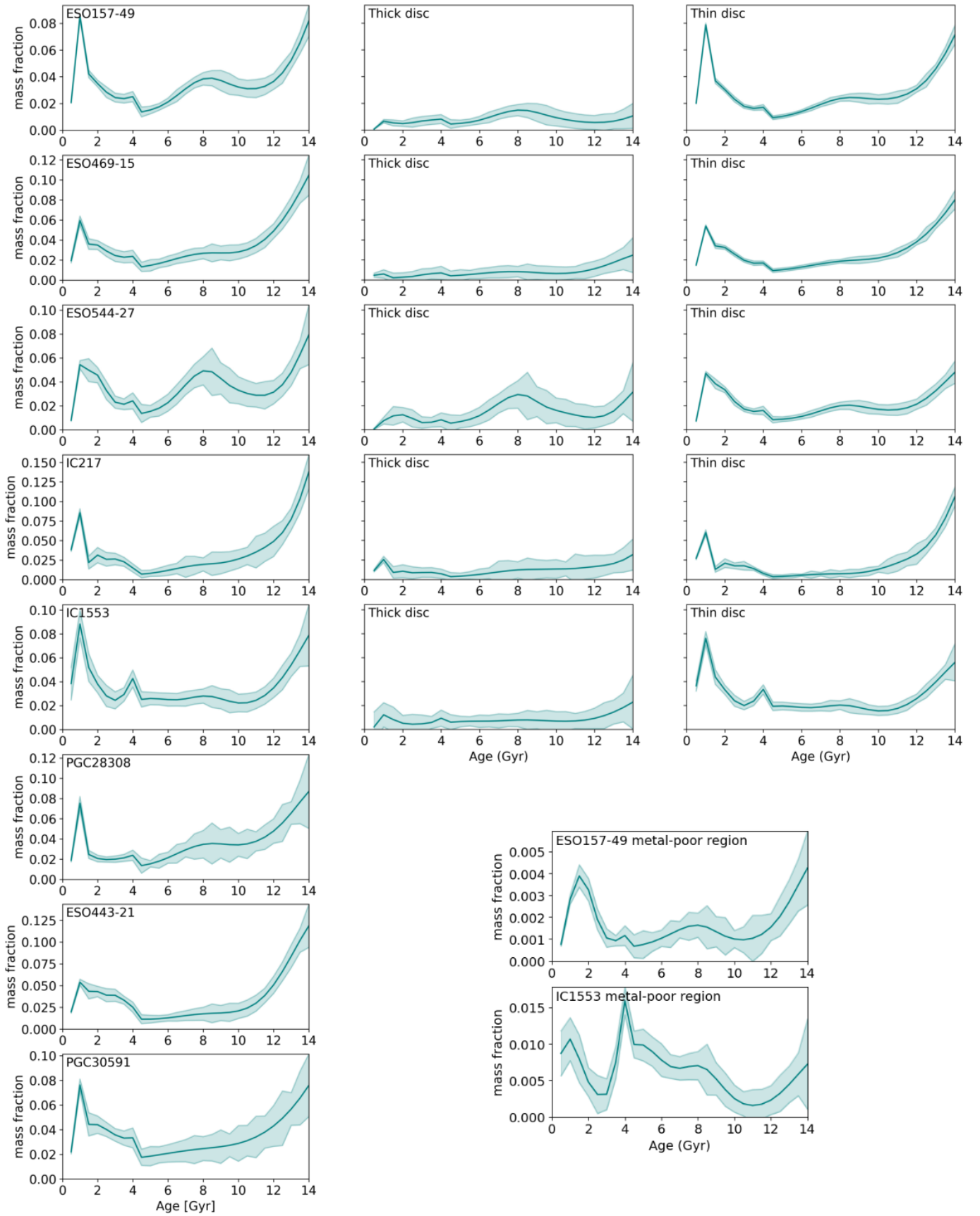


Fig. 4: Star formation histories in terms of mass fraction per age with evenly spaced age bins every 0.5 Gyr. Uncertainties from Monte Carlo simulations are shown by the shaded areas. The left column shows the star formation histories for the full covered regions of the galaxies, while the middle and right columns show the thick and thin disc respectively for the five out of the eight galaxies containing two well-defined disc components (they share the same y-axis with the left column). The additional separate panels on the lower right corner show the star formation histories of the metal-poor regions for ESO 157-49 and IC 1553.

However, metallicity and [Mg/Fe]-abundances for different ages had large uncertainties and we decided to show only the mass fractions here. This might be due to the quality of the data, the presence of a large mass fraction of young stars for which chemical properties are more difficult to determine (see also discussion in [Sattler et al. 2023](#)), combined with age-metallicity degeneracy (this degeneracy is discussed in App. A).

6. Discussion

6.1. Thin and thick discs in comparison with other edge-on galaxies

This is the first systematic study with integral-field spectroscopy of thick and thin discs in very late-type galaxies. We analyzed a sample of eight edge-on galaxies of which five have distinct thick and thin discs. Our results showed thin discs that are mostly younger, more metal-rich (except for IC 217) and less enhanced in their [Mg/Fe]-abundance than thick discs. This behavior was found in most observed thin and thick discs (see Sect. 1). However, compared to previous studies on earlier-type galaxies, ages are shifted towards young stars and differences between thin and thick discs in the stellar population parameters are lower in our sample. While lenticular galaxies were found to have a very old, metal-poor and α -enhanced thick disc and a metal-rich thin disc that can be significantly younger (but not necessarily, [Comerón et al. 2016](#); [Pinna et al. 2019b,a](#)), there are very few integral-field spectroscopy studies of stellar populations in edge-on spiral galaxies published to date, covering thick disc-dominated regions. As spiral galaxies, both NGC 5746 ([Martig et al. 2021](#)) and ESO 533-4 ([Comerón et al. 2015](#)) showed an old thick disc (~ 10 Gyr or older) and a much younger thin disc. NGC 3501, a late-type spiral galaxy with no morphological distinction between a thick and a thin disc in the observed region, displayed interesting features different from what was previously found. These were overall young ages and low metallicities, with a small thinner disc forming in the inner region of the midplane ([Sattler et al. 2023](#)).

The galaxies in our sample are somehow different from previously studied edge-on galaxies, since they are gas-rich very late-type galaxies, with very strong emission lines and extraplanar ionized gas covering the thick-disc region ([Comerón et al. 2019](#); [Rautio et al. 2022](#)). Our stellar population results show that these galaxies are systematically younger than most edge-on galaxies previously observed with integral-field spectroscopy. The thin discs in our study are very young (younger than ~ 2 Gyr). Also, the thick discs show relatively young ages (on average ~ 4 Gyr in Fig. 3 with only a few Voronoi bins reaching ≥ 8 Gyr), which are interestingly similar to thin discs in other galaxies (e.g. [Martig et al. 2021](#)). Such relatively young thick discs in spiral galaxies, with a small age difference from the thin discs, were not mapped before with integral-field spectroscopy, while some long-slit studies found hints of such thick disc ages in late-type spirals (e.g. [Yoachim & Dalcanton 2008a](#)). If we compare thick disc ages measured in this work to the ones of more massive galaxies, they seem to qualitatively agree with the predictions made for late-type galaxies in [Comerón \(2021\)](#), where thick disc ages are younger for less-massive galaxies.

Differences in metallicity and [Mg/Fe]-abundance between thick and thin discs are not sharp in our sample. These galaxies are overall metal-poor and their thin discs have nearly solar metallicities, lower than earlier-type galaxies in prior studies (super-solar in [Pinna et al. 2019b,a](#); [Martig et al. 2021](#)). Low metallicities are characteristic of very late-type galaxies and their thick and thin discs ([Yoachim & Dalcanton 2008a](#); [Comerón et al. 2015](#)).

Moreover, our thick discs are also not as [Mg/Fe]-enhanced as the four earlier-type galaxies for which spatially resolved [Mg/Fe] was measured ([Pinna et al. 2019b,a](#); [Martig et al. 2021](#)).

6.2. Formation and evolution of thick and thin discs

The combination of young ages with low metallicities and low [Mg/Fe]-abundances in the thick discs suggests a slow evolution extended in time. Star formation histories of ESO 157-49 and ESO 544-27 show that these galaxies had an intense star formation episode in their thick disc around 8 Gyr ago. This also happened in the metal-poor regions of ESO 157-49 and IC 1553, while the latter experienced its strongest star formation peaks extended over a longer period, between ~ 4 and ~ 8 Gyr ago. ESO 469-15 and IC 217, rather show a smoother star formation history in their thick discs, with a small stellar component around 6-8 Gyr. Thus, we found stellar populations formed around 7-11 Gyr ago in all thick discs in our sample, although more or less significant depending on the galaxy. There might have been an event around 8 Gyr ago which potentially contributed to the formation of the thick disc and the prominent two-disc structure. Some possible mechanisms could be mergers with satellites ([Brook et al. 2004](#); [Quinn et al. 1993](#); [Abadi et al. 2003](#)) or gas accretion from companions (e.g. for ESO 157-49, see below) or the intergalactic medium. The stellar kinematics of our sample presented in [Comerón et al. \(2019\)](#), suggested that star accretion from satellite galaxies is not the main driver of the thick disc formation. No galaxy shows signs of a retrograde stellar component larger than 10 %, but this does not rule out the accretion of a small fraction of stars. Also, a small retrograde component does not exclude the formation of thick discs from interactions or mergers with other stellar systems, as prograde mergers are favored due to dynamical friction ([Comerón et al. 2019](#)). As mentioned in Sect. 1 and different to our sample, the thick discs in [Pinna et al. \(2019b,a\)](#) and [Martig et al. \(2021\)](#) accreted around 30 % of their mass during a merger event. So there might be the possibility that the thick discs in the sample of this study are different from those of S0 galaxies in clusters ([Pinna et al. 2019b,a](#)), or the method used in [Comerón et al. \(2019\)](#) was less sensitive to the detection of accreted stellar mass.

In fact, in this sample of late-type spiral galaxies, which are overall young and gas rich, different star formation peaks might be related to different episodes of gas accretion. Star formation at the youngest ages (younger than 4 Gyr) is present in all galaxies, even in the thick disc regions, and significantly more enhanced in their thin discs. Thereby, IC 1553 has the highest SFR = 0.96 M_{\odot}/yr among the galaxies with distinct thin and thick discs (see Tab. 1, [Rautio et al. 2022](#)). Star formation in the last few Gyrs was also found by [Zaragoza-Cardiel et al. \(2020\)](#), see also Sect. 2) for IC 217 and IC 1553. Moreover, [Rautio et al. \(2022\)](#) observed vertical rotation lags of the ionized gas for ESO 157-49, ESO 544-27, IC 217 and IC 1553, and proposed gas accretion to explain them. [Keeney et al. \(2013\)](#) and [López-Cobá et al. \(2020\)](#) found signs of a galactic fountain and outflows for ESO 157-49. Therefore, gas accretion might be responsible for recent star formation events, that are primarily present in the thin discs. Putting all of this together, we propose that most thick disc stars formed in the same galaxies during a phase of intense star formation that might have peaked around old and intermediate ages (7-11 Gyr ago). This scenario was proposed by [Brook et al. \(2004\)](#) and supported by [Yu et al. \(2021\)](#), showing that every galaxy experiences a period of intense turbulent star formation in its earlier stages. During this early bursty phase, the orbits of the stars tend to be in a thicker configuration,

either because of dynamical heating (Quinn et al. 1993; Abadi et al. 2003; Elmegreen & Elmegreen 2006) or because of their formation from dynamically hot gas (Comerón et al. 2014). This bursty phase is then followed by a more stable phase in which a prominent thin disc is established. Even though the thin disc forms stars at all times, the continuous star formation until recent times is the main driver for its younger, more metal-rich and less [Mg/Fe]-enhanced stellar populations.

The metal-poor regions of the two galaxies ESO 157-49 and IC 1553 (Sect. 4.3.2) show very low metallicities and are enhanced in [Mg/Fe]-abundance compared to other regions in the thin discs. Furthermore, these metal-poor regions match spatially with regions of very high H α emission in Rautio et al. (2022) and González-Díaz et al. (2024), and could indicate intense ongoing star formation from metal-poor gas. However, we do not find stars that are significantly younger in this region than in the surroundings. We tested if the age-metallicity degeneracy could be responsible for Ppxf interpreting very young stars as being extremely metal-poor (Appendix A). This was done by plotting SSP templates of different ages and metallicities (Fig. A.1) and comparing the strength of different age- and metallicity-sensitive absorption lines. From this, we see that younger ages and lower metallicities have a similar impact on the H β line (making the absorption more intense) and the magnesium and iron lines (making them less intense). However, differences between the observed spectra of the metal-poor region and the spectra of a region with higher metallicity suggest that the stars have different properties in these regions. We also see in Fig. A.2 that the magnesium and iron lines of the observed spectra in the metal-poor region are less intense than for observed spectra in a comparable region with higher metallicity, while the age-sensitive H β absorption line has a similar intensity for both regions. This suggests that those stars are in fact more metal-poor and Ppxf is interpreting the difference between spectra correctly as a difference in metallicity. Nevertheless, the intense H α emission in these regions suggests that the stars in the metal-poor regions are also very young. We cannot recover these small age differences with our method since these metal-poor regions are surrounded by stars that are already young and age differences might be smaller or of the order of age uncertainties.

Rautio et al. (2022) proposed that ESO 544-27 has relatively older stellar populations than the other four galaxies with well-defined thin and thick discs. This galaxy falls into the green valley and shows lower H α intensities. However, these small differences at very young ages (below a hundred Myr) are within our uncertainties and are not clear in our maps. Somawanshi et al. (2024) extracted mass-weighted stellar populations of ESO 544-27 with a similar method to what is presented here. Nevertheless, they used a different setup for Ppxf, a different SSP library, and a different approach for the extinction correction, leading to large differences in this correction. Also, while we fitted the emission lines of ESO 544-27, these got masked in their study. Moreover, with a SNR-threshold of 3, they cover mostly the morphological thin disc, since the transition to the thick disc happens at about 4 arcsec from the midplane according to the definition we used here (from Comerón et al. 2018, see Sect. 2.1). Somawanshi et al. (2024) also used a different definition of thin and thick discs, based solely on their own $[\alpha/\text{Fe}]$ map. They found remarkably old ages for a galaxy with current star formation. These old ages are uniform in the galaxy, with no clear differences at various distances from the midplane. In fact, stars on the midplane look even slightly older (≥ 10 Gyr) than

off-plane (~ 9.95 Gyr) in their age map. In our work, we do not find such old stellar populations in this galaxy. As mentioned above, all galaxies in our sample show very young ages. While Somawanshi et al. (2024) did not find a clear vertical metallicity gradient, in a region that corresponds mostly to our thin disc, their values in that same region they analyzed are similar to what we obtained. Contrary to us, they found $[\alpha/\text{Fe}]$ enhancement at larger distances from the midplane, with a low- $[\alpha/\text{Fe}]$ thin disc in the midplane region. The above-mentioned differences in the method could be responsible for the discrepancies between their results and our results in e.g. the age maps.

6.3. Thin and thick disc masses

All galaxies with distinct thin and thick discs show a larger mass fraction in the thin-disc dominated region (around 61 to 77 %) than in the thick-disc dominated region (around 22 to 39 %), as shown in Tab. 4. Comerón et al. (2018) calculated thin and thick disc masses (respectively, M_t and M_T in Tab. 1). M_t are around 59 to 68 % and M_T are 32 to 41 % of the total galaxy stellar mass. This discrepancy in the mass fractions comes from the different methods and the different wavelength ranges that were used. While we used the optical range, where a larger amount of light is obscured by the dust, Comerón et al. (2018) used images in the infrared. This wavelength range is less affected by the dust than MUSE wavelength range, and this affects mostly the mass of the thin disc, where the dust is located. More importantly, we calculated our mass fractions from restricted regions covered by the Voronoi bins since the MUSE pointings did not cover the full galaxies. The Spitzer S⁴G (Sheth et al. 2010) images used in Comerón et al. (2018), on the other hand, cover the entire galaxies. In particular, we possibly cover a smaller fraction of the faint thick disc than S⁴G data, resulting in a smaller thick disc mass fraction and a larger thin disc fraction. Further, Comerón et al. (2018) assumed a fixed mass-to-light ratio for the thin and the thick disc, while our mass-to-light ratios vary for different Voronoi bins (with different combinations of SSP models). Even if this is a second order effect, the choice of a mass-to-light ratio has an important impact on the mass estimates. Another reason why the predictions are different is that all the light above a certain height is assigned to the thick disc and all the light below it is assigned to the thin disc. But at all heights there is a contribution from both discs. So even though the thin disc dominates the surface brightness close to the midplane, a significant fraction of the thick disc total mass is hiding there. While we calculate thick and thin disc masses only in the region where they dominate, Comerón et al. (2018) used mass profiles that extend, for each disc, to the full vertical coverage of the data. Therefore, the thick disc mass fractions provided in our work are underestimated. Despite this discrepancy in mass to Comerón et al. (2018), the thin discs in the sample clearly host a much larger mass than the thick disc (almost a factor of two larger, according to both our results and Comerón et al. 2018). As most of the galaxies have circular velocities ≥ 90 km s⁻¹, this distribution of thin and thick disc masses corresponds well with the findings of Yoachim & Dalcanton (2006) mentioned in Sect. 1, where they predicted that thick discs are usually less massive than thin discs.

6.4. Galaxies with one dominating disc

The galaxies with only one dominating disc component (especially ESO 443-21 and PGC 30591), show slightly different star formation histories from galaxies with two distinct components. The

intermediate aged stellar population component (see Sect. 6.2) is not as pronounced, and they rather show a more continuous decrease along those ages (10-6 Gyr). This difference, compared to galaxies with a distinct thick disc, suggests that a phase of intense star formation peaking at intermediate ages might support the formation of a prominent thick disc in the late-type spirals of our sample. Moreover, these three galaxies show a recent star forming burst at very young ages (younger than 2-4 Gyr), similar to thin discs in the sample. These results are in agreement with Zaragoza-Cardiel et al. (2020, see also Sect. 2), who detected star formation in the last Gyr for PGC 28308, ESO 443-21 and PGC 30591. This suggests a similar recent formation history for these gas-rich and young galaxies, where gas accretion is probably playing a role. In fact, previous studies showed signs of interactions and gas accretion in some galaxies. PGC 28308 has disturbed gaseous outskirts and forms a pair with MCG-02-25-019 (see Sect. 2, Tully et al. 2009; Meyer et al. 2004). So dynamical interactions with the paired galaxy might be responsible for the disturbances and the recent increase in star formation. These disturbances might also have brought existing stars into dynamically hotter orbits contributing to the mass assembly of the thick disc component. Also, ESO 443-21 was classified by Schwarzkopf & Dettmar (2000) as an interacting/merging candidate. Together with a negative radial metallicity gradient (Fig. 3), we suggest that this galaxy is growing a thin disc structure from the “inside-out” that might become more pronounced in the future. This is similar to NGC 3501 where the presence of a metal-rich inner thin disc in the midplane suggested an on-going “inside-out” formation of a future prominent thin disc (Sattler et al. 2023). However, we can only speculate about the growth of a prominent future thin disc, and the development of distinct thin and thick discs during the evolution might not hold for all galaxies. On the other hand, these single-disc galaxies may already have two distinct disc components in reality, that are just not detected because of a slightly lower inclination angle (not perfectly edge-on) compared to the other galaxies. Especially in low-mass galaxies the absence of well-defined and thin dust lanes makes it difficult to ensure an edge-on orientation of the galaxy. So some of these single-disc galaxies might not show well-defined thick and thin discs because they are not perfectly edge-on (see Fig. 9 in Comerón et al. 2011). This would explain why differences in the stellar populations are displayed between the midplane region and regions at larger heights.

7. Summary and conclusion

In this study, we used the MUSE data of eight late-type galaxies from Comerón et al. (2019) to derive their stellar populations (age, metallicity and [Mg/Fe]-abundance) and the star formation histories. This is the first systematic stellar population mapping of a sample of edge-on very late-type galaxies, gas-rich and with extraplanar ionized gas. In this type of galaxies, we find younger ages and lower metallicities in both thick and thin discs than previously found in earlier-type disc galaxies. While thick discs do not show the typical α -enhancement formerly seen in other edge-on galaxies, they are systematically younger than previously found, with ages that were traditionally associated to thin discs in earlier-type galaxies (e.g. Pinna et al. 2019a; Martig et al. 2021). Differences between thick and thin discs in our sample are rather small, suggesting a slower and more continuous upside-down formation than in prior studied earlier-type galaxies. Our star formation histories show that a phase of intense star formation (potentially with minor mergers and gas accretion) lasting until around 7 to 8 Gyr might support the formation of

a thick disc. We detected a variety of intermediate and older stars in the thick discs star formation histories, which might be suggesting that this intense phase heated stars from the midplane leaving a variety of ages in thicker orbits. This was observed in the stellar population maps, where the thick discs tend to be more metal-poor and more enhanced in the [Mg/Fe]-abundance than the thin discs. For the thin discs in this sample, we saw in the star formation histories an increase in the mass fraction of the youngest stars compared to intermediate ages, which seems to not appear in the thick discs. So we suggest that after an intense and likely turbulent star formation phase, a more steady phase begins in which the thin disc is established by continuous and efficient star formation, probably fueled by gas accretion. In galaxies with only one dominating disc component, we did not see a pronounced intermediate aged stellar population, but rather a more continuous decrease along 10 to 6 Gyr. Similar to the galaxies with well-defined thin and thick discs, the single-disc galaxies also had star formation bursts at very young ages. We proposed that on-going star formation together with dynamical interactions in these galaxies might form more enhanced thin disc components in the future. But it was also discussed that far from edge-on inclination could hide a already established two-disc structure in these galaxies. Nor does it have to be universally true that all galaxies eventually develop distinct thin and thick discs during their evolution.

To conclude, this work is the first attempt to unveil the formation and evolution of thin and thick discs in very young, dusty and gaseous edge-on spiral galaxies, with a spatially resolved stellar population analysis. However, more work needs to be done in this field to gain a better understanding of the thick and thin disc formation in spiral galaxies. In addition, by testing other SSP models and fitting codes for the stellar populations, a better understanding of the current systematics can be achieved. In the future, larger surveys of edge-on galaxies like GECKOS⁶ (van de Sande et al. 2023) will help to disentangle the leading formation mechanisms of thick and thin discs.

Acknowledgements. NS acknowledges support from the Deutsche Forschungsgemeinschaft (DFG, German Research Foundation) – Project-ID 138713538 – SFB 881 (“The Milky Way System”, subproject B08) and from the Deutsche Forschungsgemeinschaft (DFG, German Research Foundation) in the form of an Emmy Noether Research Group (grant number KR4598/2-1, PI Kreckel) and the European Research Council’s starting grant ERC StG-101077573 (“ISM-METALS”). FP acknowledges support from the Agencia Estatal de Investigación del Ministerio de Ciencia e Innovación (MCIN/AEI/ 10.13039/501100011033) under grant (PID2021-128131NB-I00) and the European Regional Development Fund (ERDF) “A way of making europe”. FP acknowledges support also from the Horizon Europe research and innovation programme under the Marie Skłodowska-Curie grant “TraNSLate” No 101108180. IMN and JFB acknowledge support from the PID2022-140869NB-I00 grant from the Spanish Ministry of Science and Innovation.

References

- Abadi, M. G., Navarro, J. F., Steinmetz, M., & Eke, V. R. 2003, *ApJ*, 597, 21
 Abbott, T. M. C., Adamów, M., Aguena, M., et al. 2021, *ApJS*, 255, 20
 Bacon, R., Accardo, M., Adjali, L., et al. 2010, in *Society of Photo-Optical Instrumentation Engineers (SPIE) Conference Series*, Vol. 7735, *Ground-based and Airborne Instrumentation for Astronomy III*, ed. I. S. McLean, S. K. Ramsay, & H. Takami, 773508
 Bacon, R., Conseil, S., Mary, D., et al. 2017, *A&A*, 608, A1
 Baldwin, J. A., Phillips, M. M., & Terlevich, R. 1981, *PASP*, 93, 5
 Boecker, A., Leaman, R., van de Ven, G., et al. 2020, *MNRAS*, 491, 823
 Bournaud, F., Elmegreen, B. G., & Martig, M. 2009, *ApJ*, 707, L1
 Brook, C. B., Kawata, D., Gibson, B. K., & Freeman, K. C. 2004, *ApJ*, 612, 894
 Burstein, D. 1979, *ApJ*, 234, 829

⁶ <https://geckos-survey.org/index.html>

- Cappellari, M. 2017, *MNRAS*, 466, 798
- Cappellari, M. 2022, arXiv e-prints, arXiv:2208.14974
- Cappellari, M. & Copin, Y. 2003, *MNRAS*, 342, 345
- Cardelli, J. A., Clayton, G. C., & Mathis, J. S. 1989, *ApJ*, 345, 245
- Casagrande, L., Silva Aguirre, V., Schlesinger, K. J., et al. 2016, *MNRAS*, 455, 987
- Chambers, K. C., Magnier, E. A., Metcalfe, N., et al. 2016, arXiv e-prints, arXiv:1612.05560
- Comerón, S. 2021, *A&A*, 645, L13
- Comerón, S., Elmegreen, B. G., Knapen, J. H., et al. 2011, *ApJ*, 741, 28
- Comerón, S., Elmegreen, B. G., Salo, H., et al. 2012, *ApJ*, 759, 98
- Comerón, S., Elmegreen, B. G., Salo, H., et al. 2014, *A&A*, 571, A58
- Comerón, S., Salo, H., Janz, J., Laurikainen, E., & Yoachim, P. 2015, *A&A*, 584, A34
- Comerón, S., Salo, H., & Knapen, J. H. 2018, *A&A*, 610, A5
- Comerón, S., Salo, H., Knapen, J. H., & Peletier, R. F. 2019, *A&A*, 623, A89
- Comerón, S., Salo, H., Peletier, R. F., & Mentz, J. 2016, *A&A*, 593, L6
- Conroy, C., Weinberg, D. H., Naidu, R. P., et al. 2022, arXiv e-prints, arXiv:2204.02989
- Domínguez-Gómez, J., Pérez, I., Ruiz-Lara, T., et al. 2023, arXiv e-prints, arXiv:2306.16818
- Elmegreen, B. G. & Elmegreen, D. M. 2006, *ApJ*, 650, 644
- Emsellem, E., Schinnerer, E., Santoro, F., et al. 2022, *A&A*, 659, A191
- Falcón-Barroso, J., Sánchez-Blázquez, P., Vazdekis, A., et al. 2011, *A&A*, 532, A95
- Flewelling, H. A., Magnier, E. A., Chambers, K. C., et al. 2020, *ApJS*, 251, 7
- Freudling, W., Romaniello, M., Bramich, D. M., et al. 2013, *A&A*, 559, A96
- Gaia Collaboration, Recio-Blanco, A., Kordopatis, G., et al. 2022, arXiv e-prints, arXiv:2206.05534
- Gallart, C., Bernard, E. J., Brook, C. B., et al. 2019, *Nature Astronomy*, 3, 932
- Gilmore, G. & Reid, N. 1983, *MNRAS*, 202, 1025
- Gilmore, G. & Wyse, R. F. G. 1985, *AJ*, 90, 2015
- González-Díaz, R., Rosales-Ortega, F. F., & Galbany, L. 2024, arXiv e-prints, arXiv:2406.17123
- Grand, R. J. J., Gómez, F. A., Marinacci, F., et al. 2017, *MNRAS*, 467, 179
- Guérou, A., Emsellem, E., Krajnović, D., et al. 2016, *A&A*, 591, A143
- Hayden, M. R., Recio-Blanco, A., de Laverny, P., Mikolaitis, S., & Worley, C. C. 2017, *A&A*, 608, L1
- Ivezić, Ž., Sesar, B., Jurić, M., et al. 2008, *ApJ*, 684, 287
- Kasparova, A. V., Katkov, I. Y., & Chilingarian, I. V. 2020, *MNRAS*, 493, 5464
- Kasparova, A. V., Katkov, I. Y., Chilingarian, I. V., et al. 2016, *MNRAS*, 460, L89
- Katkov, I. Y., Kniazev, A. Y., Kasparova, A. V., & Sil'chenko, O. K. 2019, *MNRAS*, 483, 2413
- Keeney, B. A., Stocke, J. T., Rosenberg, J. L., et al. 2013, *ApJ*, 765, 27
- López-Cobá, C., Sánchez, S. F., Anderson, J. P., et al. 2020, *AJ*, 159, 167
- Magnier, E. A., Chambers, K. C., Flewelling, H. A., et al. 2020a, *ApJS*, 251, 3
- Magnier, E. A., Schlafly, E. F., Finkbeiner, D. P., et al. 2020b, *ApJS*, 251, 6
- Magnier, E. A., Sweeney, W. E., Chambers, K. C., et al. 2020c, *ApJS*, 251, 5
- Makarov, D., Prugniel, P., Terekhova, N., Courtois, H., & Vauglin, I. 2014, *A&A*, 570, A13
- Martig, M., Bournaud, F., Croton, D. J., Dekel, A., & Teyssier, R. 2012, *ApJ*, 756, 26
- Martig, M., Minchev, I., Ness, M., Fouesneau, M., & Rix, H.-W. 2016, *ApJ*, 831, 139
- Martig, M., Pinna, F., Falcón-Barroso, J., et al. 2021, *MNRAS*, 508, 2458
- Meyer, M. J., Zwaan, M. A., Webster, R. L., et al. 2004, *MNRAS*, 350, 1195
- Minchev, I., Martig, M., Streich, D., et al. 2015, *ApJ*, 804, L9
- Mo, H., van den Bosch, F. C., & White, S. 2010, *Galaxy Formation and Evolution*
- Morganson, E., Gruendl, R. A., Menanteau, F., et al. 2018, *PASP*, 130, 074501
- Muñoz-Mateos, J. C., Sheth, K., Regan, M., et al. 2015, *ApJS*, 219, 3
- Pan, Z., Li, J., Lin, W., et al. 2015, *ApJ*, 804, L42
- Peletier, R. F. 2013, in *Secular Evolution of Galaxies*, ed. J. Falcón-Barroso & J. H. Knapen, 353
- Pérez, E., Cid Fernandes, R., González Delgado, R. M., et al. 2013, *ApJ*, 764, L1
- Pinna, F., Falcón-Barroso, J., Martig, M., et al. 2019a, *A&A*, 625, A95
- Pinna, F., Falcón-Barroso, J., Martig, M., et al. 2019b, *A&A*, 623, A19
- Pinna, F., Walo-Martín, D., Grand, R. J. J., et al. 2024, *A&A*, 683, A236
- Queiroz, A. B. A., Anders, F., Chiappini, C., et al. 2020, *A&A*, 638, A76
- Quinn, P. J., Hernquist, L., & Fullagar, D. P. 1993, *ApJ*, 403, 74
- Rautio, R. P. V., Salo, H., Watkins, A. E., Comerón, S., & Venhola, A. 2024, arXiv e-prints, arXiv:2409.16062
- Rautio, R. P. V., Watkins, A. E., Comerón, S., et al. 2022, *A&A*, 659, A153
- Sánchez-Blázquez, P., Rosales-Ortega, F. F., Méndez-Abreu, J., et al. 2014, *A&A*, 570, A6
- Santucci, G., Brough, S., Scott, N., et al. 2020, *ApJ*, 896, 75
- Sarzi, M., Falcón-Barroso, J., Davies, R. L., et al. 2006, *MNRAS*, 366, 1151
- Sattler, N., Pinna, F., Neumayer, N., et al. 2023, *MNRAS*, 520, 3066
- Schlesinger, K. J., Johnson, J. A., Rockosi, C. M., et al. 2012, *ApJ*, 761, 160
- Schwarzkopf, U. & Dettmar, R. J. 2000, *A&AS*, 144, 85
- Scott, N., van de Sande, J., Sharma, S., et al. 2021, *ApJ*, 913, L11
- Sheth, K., Regan, M., Hinz, J. L., et al. 2010, *PASP*, 122, 1397
- Somawanshi, D., Bhattacharya, S., Kataria, M., & Kobayashi, C. 2024, *MNRAS*, 531, 4336
- Soto, K. T., Lilly, S. J., Bacon, R., Richard, J., & Conseil, S. 2016, *MNRAS*, 458, 3210
- Tully, R. B., Courtois, H. M., & Sorce, J. G. 2016, *AJ*, 152, 50
- Tully, R. B., Rizzi, L., Shaya, E. J., et al. 2009, *AJ*, 138, 323
- Tully, R. B., Shaya, E. J., Karachentsev, I. D., et al. 2008, *ApJ*, 676, 184
- van de Sande, J., Fraser-McKelvie, A., Fisher, D. B., et al. 2023, arXiv e-prints, arXiv:2306.00059
- Vazdekis, A., Coelho, P., Cassisi, S., et al. 2015, *MNRAS*, 449, 1177
- Wang, Z., Hayden, M. R., Sharma, S., et al. 2023, arXiv e-prints, arXiv:2310.18258
- Waters, C. Z., Magnier, E. A., Price, P. A., et al. 2020, *ApJS*, 251, 4
- Weilbacher, P. M., Streicher, O., Urrutia, T., et al. 2012, in *Society of Photo-Optical Instrumentation Engineers (SPIE) Conference Series*, Vol. 8451, Software and Cyberinfrastructure for Astronomy II, ed. N. M. Radziwill & G. Chiozzi, 84510B
- Worthey, G., Faber, S. M., & Gonzalez, J. J. 1992, *ApJ*, 398, 69
- Yoachim, P. & Dalcanton, J. J. 2006, *AJ*, 131, 226
- Yoachim, P. & Dalcanton, J. J. 2008a, *ApJ*, 683, 707
- Yoachim, P. & Dalcanton, J. J. 2008b, *ApJ*, 682, 1004
- Yu, S., Bullock, J. S., Klein, C., et al. 2021, *MNRAS*, 505, 889
- Zaragoza-Cardiel, J., Fritz, J., Aretxaga, I., et al. 2020, *MNRAS*, 499, 1172
- Zhang, H.-X., Hunter, D. A., Elmegreen, B. G., Gao, Y., & Schruha, A. 2012, *AJ*, 143, 47

Appendix A: Age-metallicity degeneracy

In this Appendix, we show the tests on the age-metallicity degeneracy of the stellar templates discussed in Sect. 6. Fig. A.1 shows a comparison of MILES SSP models having different ages, metallicities and [Mg/Fe]-abundances. The two panels at the top show templates with different ages (0.05 Gyr and 10 Gyr) and same sub-solar [M/H] (-1.49 dex), whereas the bottom panels show ages (0.05 Gyr and 10 Gyr) and super-solar [M/H] (0.40 dex). Templates having the same ages (0.05 Gyr) and different [M/H] (-1.49 dex and 0.040 dex) can be compared using the two left panels, whereas the same comparison can be done on older ages (10 Gyr) using the two right panels. Additionally, all panels show the two corresponding templates with [Mg/Fe] = 0.00 and 0.40 as black solid and red dashed curves, respectively. Comparing all the different SSP models, one can see that younger ages and lower metallicities have a similar impact on the $H\beta$ line (making the absorption more intense) and the Mg and Fe lines (making them less intense). In Fig. A.2, we further show the differences in the spectra of the metal-poor region compared to a region, at a similar radius but on the opposite side of the disc, with higher metallicity. It can be observed that the mean spectrum of the metal-poor region has less intense magnesium and iron lines than the counter-part mean spectrum, while the $H\beta$ line seems to be quite similar.

Appendix B: Tests for stellar population fitting

For the fitting of the stellar populations, we tested two different MILES SSP model selections:

- Limited set of models (as in Sattler et al. 2023) that are in the safe range⁷ and provide the same resolution in the full age range:
 - $1.26 \text{ dex} \leq \text{metallicity} \leq 0.40 \text{ dex}$, $0.5 \text{ Gyr} \leq \text{age} \leq 14 \text{ Gyr}$ evenly spaced every 0.5 Gyr, [Mg/Fe] = 0.0 and 0.4 dex
- Full range of models, with varying age resolution depending on the age range:
 - $2.27 \text{ dex} \leq \text{metallicity} \leq 0.40 \text{ dex}$, $0.03 \text{ Gyr} \leq \text{age} \leq 14 \text{ Gyr}$, [Mg/Fe] = 0.0 and 0.4 dex

together with the two different values of regularization = 1 and 10. In Fig. B.1, examples of the star formation history grids resulting from these tests are shown for ESO 443-21.

One can see that the limited models and regularization = 1 fit show peaks in star formation at 14 Gyr (bimodal in [M/H]), 8.5 Gyr ([M/H] \approx -1.26 dex) and 2 Gyr ([M/H] \approx -0.96 dex). These peaks are smoother for the limited set of models and regularization = 10 fit, but remain around the same ages and metallicity. Using the full range of models, SSPs of lower metallicities are selected for the best fit by PPF. This suggests that, when using the restricted set of models (with [M/H] \geq -1.26 dex) PPF is hitting the boundaries of low metallicities. This explains why when the [M/H] \leq 1.49 dex SSP models are added, they are used by PPF for the fitting. Therefore, we need these lower metallicity models to properly fit the metal-poor peaks. Also, the star formation history is overall smoother in the bottom panels (full set of models) than the top panels (limited model grid) for the same regularization, and the 8.5 Gyr peak is less pronounced but still noticeable. For the full range of models and regularization = 10, the star formation peaks are even smoother and the 8.5 Gyr peak is very hard to detect. So the same regularization has a stronger effect when we use this set

Table C.1: Average uncertainties for the mass-weighted stellar population maps calculated as the mean uncertainty of all bins belonging to the corresponding component.

Galaxy	Component	ΔAge [Gyr]	$\Delta[\text{M}/\text{H}]$ [dex]	$\Delta[\text{Mg}/\text{Fe}]$ [dex]
ESO 157-49	thin disc	0.95	0.09	0.13
	thick disc	1.99	0.12	0.15
ESO 469-15	thin disc	1.06	0.09	0.13
	thick disc	2.63	0.28	0.24
ESO 544-27	thin disc	1.03	0.09	0.10
	thick disc	1.87	0.15	0.15
IC 217	thin disc	1.05	0.14	0.14
	thick disc	2.03	0.14	0.17
IC 1553	thin disc	3.24	0.40	0.37
	thick disc	5.04	0.57	0.26
PGC 28308	full galaxy	0.78	0.06	0.18
ESO 443-21	full galaxy	1.40	0.15	0.22
PGC 30591	full galaxy	1.00	0.10	0.13

of models. Finally, we decided to use the full range of MILES SSP models and regularization = 1 for the full sample.

Appendix C: Mass-weighted stellar populations

Here we present the mass-weighted stellar population maps in Fig. C.1.

Comparing the light- and mass-weighted stellar population maps, the mass-weighted ones show on average older ages, higher metallicities and lower [Mg/Fe]-abundances (also seen in Sánchez-Blázquez et al. 2014; Sattler et al. 2023). This difference in age is because younger stars contribute more to the light-weighted results due to their higher luminosity compared to older stars. In contrast, older stars contribute to a larger mass, leading to more prominence in mass-weighted results. As a consequence, the light-weighted map tends to exhibit younger average ages compared to the mass-weighted map. Further, as indicated in Tab. C.1, the mass-weighted stellar population properties show larger uncertainties on average compared to the light-weighted ones.

Appendix D: Uncertainties for light-weighted stellar populations

In Fig. D.1 we show the uncertainties of the light-weighted stellar populations as derived by Monte Carlo simulations described in Sect. 4.3.3. In general, the uncertainties for all galaxies are smaller in the midplane region and get larger for regions farther away, which is explained by the lower SNR per Voronoi bin and also per pixel before even Voronoi binning these regions. Tab. 3 contains a summary of the average uncertainties for each galaxy in light-weighted age, metallicity and [Mg/Fe]-abundances.

⁷ <http://research.iac.es/proyecto/miles/pages/ssp-models/safe-ranges.php>

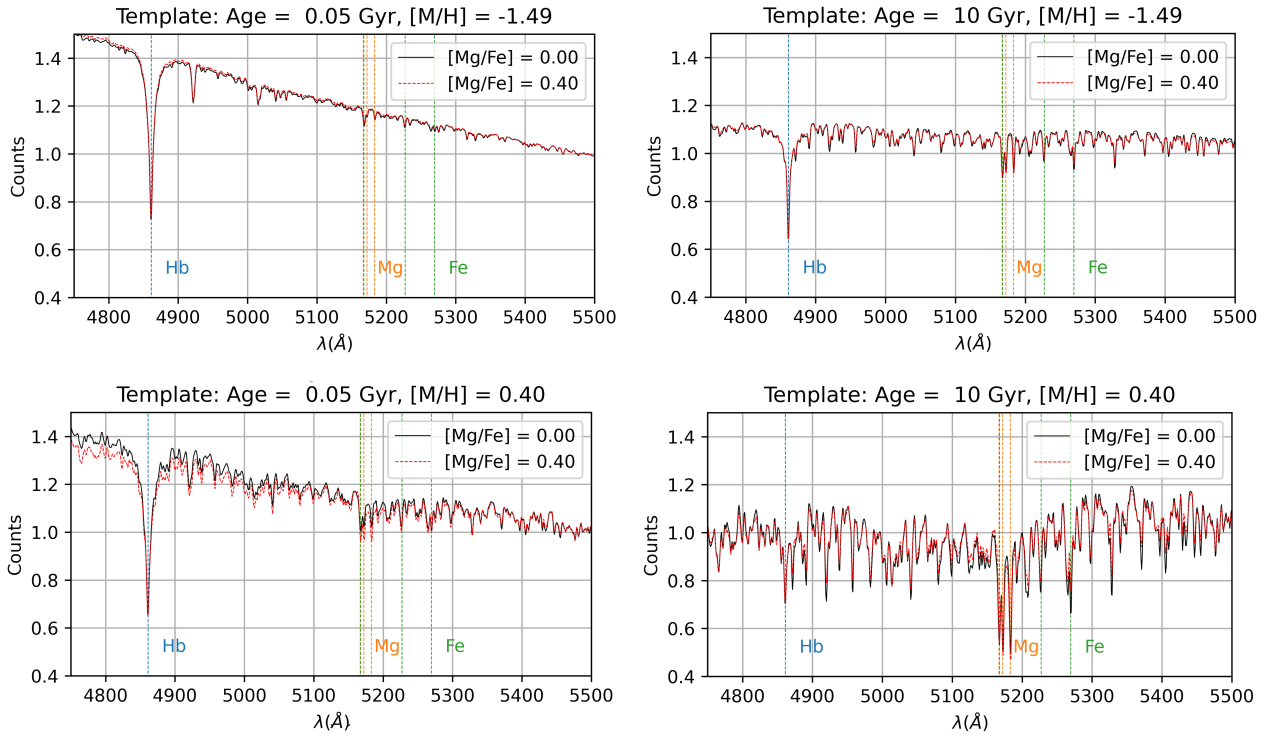


Fig. A.1: Comparison of MILES SSP templates with different ages (0.05 and 10 Gyr, from left to right) and metallicities (-1.49 and 0.40 dex, from top to bottom). The templates are shown for both values of [Mg/Fe] (black: 0.00 dex, red: 0.40 dex) and important absorption features are indicated by colored dashed lines (blue: H β at 4861.33 Å, orange: Mg at 5183, 5172 and 5167 Å, green: Fe at 5167.49, 5227.15 and 5269.54 Å).

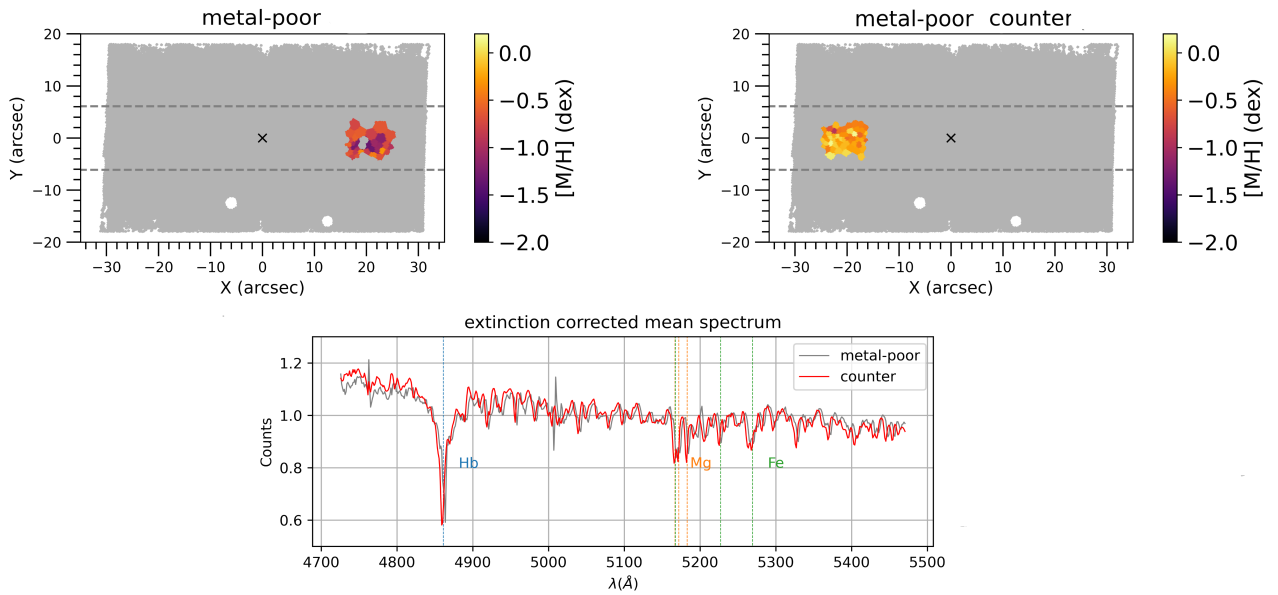


Fig. A.2: Comparison of the extinction corrected mean spectra of the metal-poor region (grey) and a counter-part region (red) on the other side of the center for ESO 157-49.

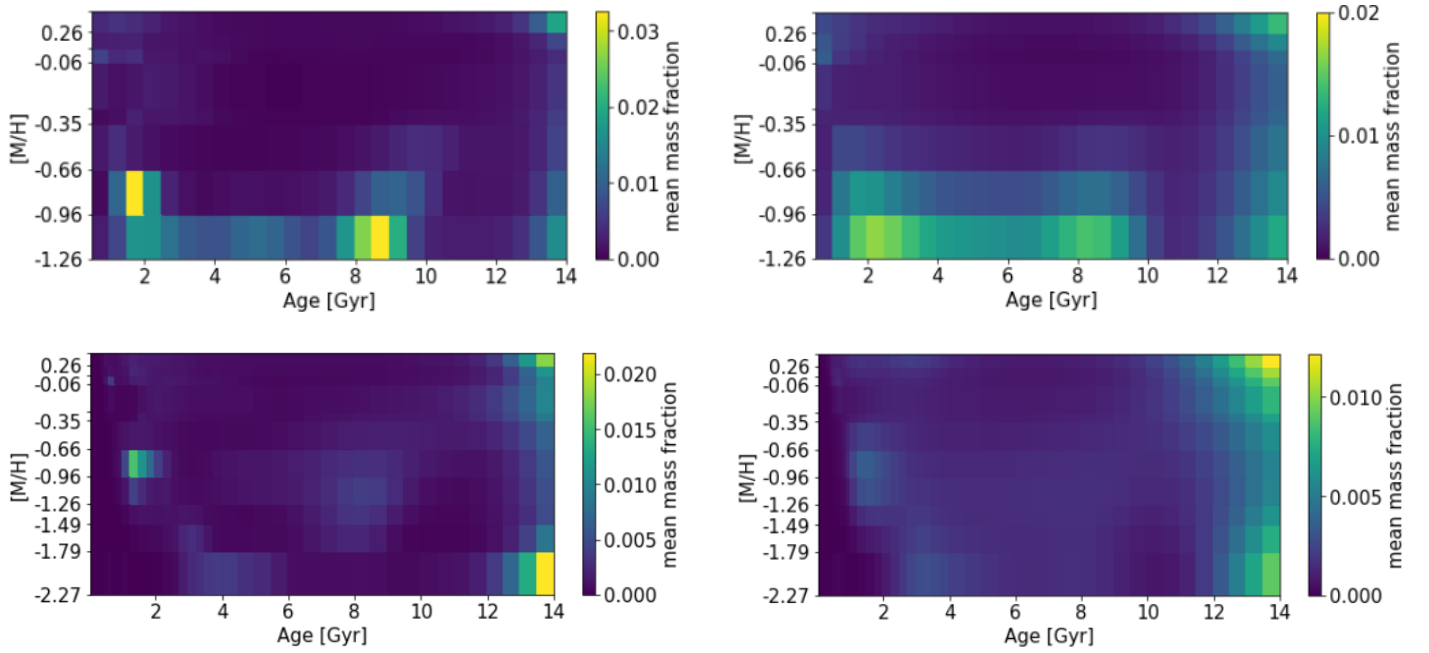


Fig. B.1: Star formation history tests for one central Voronoi bin of ESO 443-21. In a metallicity-age grid, we show for this Voronoi bin the color-coded mass fraction assigned to different ages and metallicities summed up for both values of $[Mg/Fe]$ ($= 0.0$ and 0.40 dex) The top figures show the results using limited models and a regularization $= 1$ (left) / 10 (right). The bottom figures show the results for the full range of models and a regularization $= 1$ (left) / 10 (right).

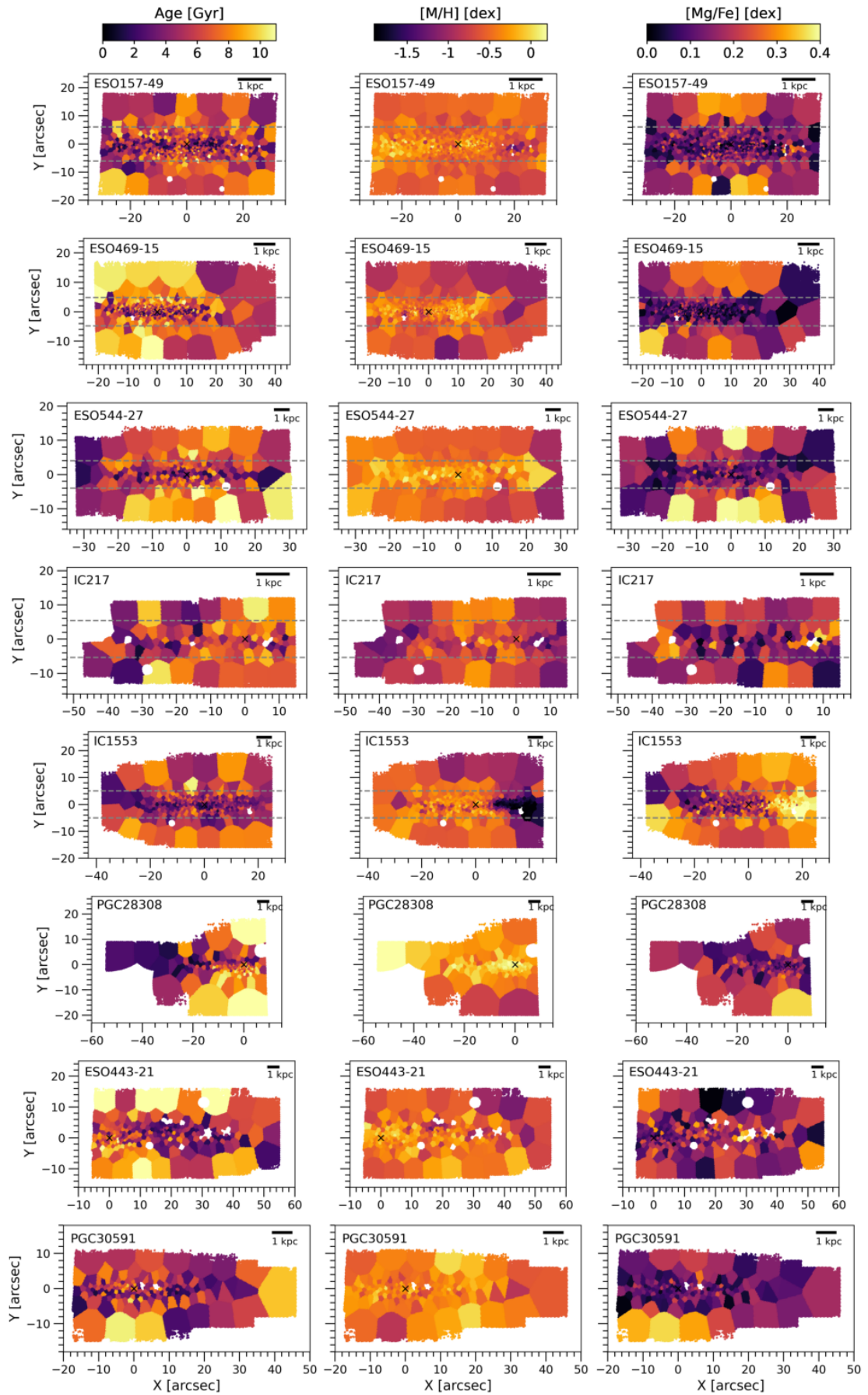


Fig. C.1: Mass-weighted age (left), metallicity (middle) and [Mg/Fe]-abundance (right) maps for the full sample. Grey dashed lines mark the regions above and below which the thick disc dominates the vertical surface-brightness profiles.

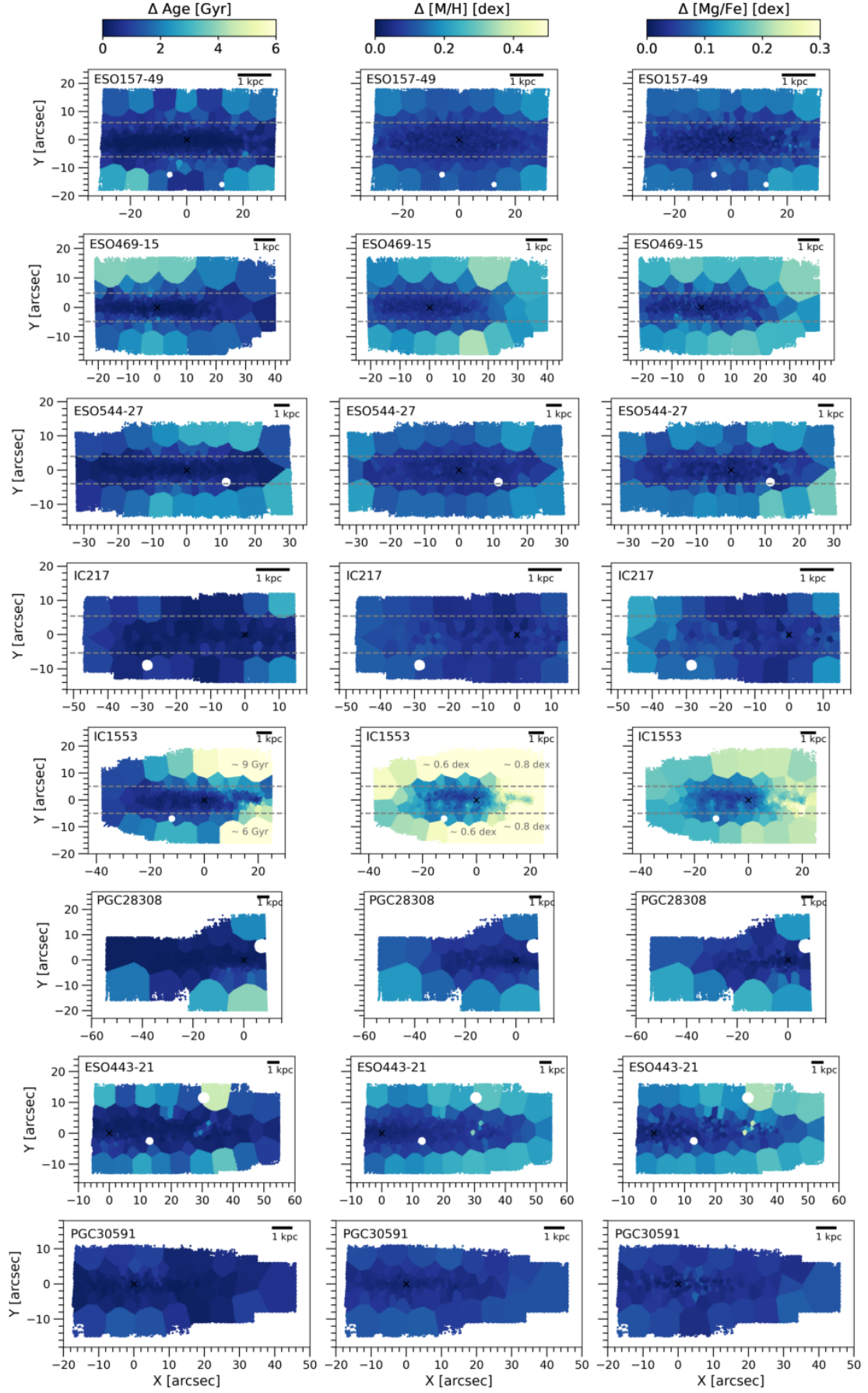


Fig. D.1: Uncertainties of the light-weighted age (left), metallicity (middle) and [Mg/Fe]-abundance (right) maps for the full sample. For IC 1553, when the color scale saturates, we indicated the approximate uncertainty in the Voronoi bins by numbers. Grey dashed lines mark the regions above and below which the thick disc dominates the vertical surface-brightness profiles.